DOCUMENT RESUME

ED 161 705 SE 025 159

TITLE	Minicourses in Astrophysics, Modular Approach, Vol. I.
INSTITUTION	Illinois Univ., Chicago.
SPONS AGENCY	National Science Foundation, Washington, D.C.
BUREAU NO	SED-75-21297
PUB DATE	77
NOTE	144p.; For related document, see SE 025 160; Contains occasional light and broken type
EDRS PRICE	MF-$0.83 HC-$7.35 Plus Postage.
DESCRIPTORS	*Astronomy; *Curriculum Guides; Evolution; Graduate Study; *Higher Education; *Instructional Materials; Light; Mathematics; Nuclear Physics; *Physics; Radiation; Relativity; Science Education; *Short Courses; Space Sciences
IDENTIFIERS	*Astrophysics

ABSTRACT

This is the first volume of a two-volume minicourse in astrophysics. It contains chapters on the following topics: planetary atmospheres; X-ray astronomy; radio astrophysics; molecular astrophysics; and gamma-ray astrophysics. Each chapter gives much technical discussion, mathematical treatment, diagrams, and examples. References are included with each chapter. (BB)

MINICOURSES IN ASTROPHYSICS
MODULAR APPROACH
VOL. I

DEVELOPED AT THE
UNIVERSITY OF ILLINOIS AT CHICAGO
1977

SUPPORTED BY NATIONAL SCIENCE FOUNDATION

DIRECTOR: S. SUNDARAM
DEPARTMENT OF PHYSICS
UNIVERSITY OF ILLINOIS
CHICAGO, ILLINOIS 60680

ASSOCIATE DIRECTOR: J. BURNS
DEPARTMENT OF PHYSICS AND SPACE SCIENCES
FLORIDA INSTITUTE OF TECHNOLOGY
MELBOURNE, FLORIDA 32901

PLANETARY ATMOSPHERES

1. Introduction

The study of the planets and the solar system is one of the most important and oldest of the various branches of astrophysics. With renewed interest on the part of the scientists and engineers during the sixties and the early seventies on various space programs, this study of solar system and the exploration of the possible existence of life on other planets besides earth has occupied the major thrust of all programs. As we know, the programs are still continuing and with more and more sophisticated instrumentation, the healthy competition and cooperation between the U.S. and U.S.S.R. can be hoped to further our understanding of the solar system in detail.

Let us begin our discussion with the general ideas concerning the formation of the planets and the evolution of planetary atmospheres. Beginning with the "Big Bang" of our expanding universe some nearly ten billion years ago, the continuous burning of hydrogen has yielded the helium in the universe and hydrogen as well as helium are by far the most abundant elements in the universe. In the interiors of the stars, the continuous burning besides yielding helium also leads to the final nuclear reactions in the last stages of nuclear burning when the temperature rises to $\sim 10^9$ °K. The final nuclear reactions take place so fast that the resulting explosion ejects a major part of the star into

interstellar space thus leading to the enrichment of heavy elements in the galactic matter.

The solar system which is approximately five billion years old traces its origin to the nebula and the vastly enhanced solar wind in the early stages of sun's life must have influenced the nature of the gaseous matter in the planets. The inner planets of Mercury, Venus, Earth, and Mars have only a small fraction of their total initial mass and very little of hydrogen and helium whereas the outer planets of Jupiter, Saturn, Uranus, and Neptune are much more massive and retain a composition very similar to the initial nebula. In this evolutionary process from the primordial nebula, it is interesting to note how the analysis of ancient rocks on earth gives us clues to the beginnings of life on earth. The early atmosphere of earth was mainly H_2, CH_4, N_2, NH_3, CN, CO, and H_2O. Aminoacids and organic substances were formed from these constituents. The organic chemicals at the bottoms of the lakes and oceans through different reactions formed DNA, RNA and others like the various enzymes and thus leading to photosynthesis with the vitally needed oxygen as a by-product. Finally, the protective ozone also was formed from oxygen. In the next section, we shall review very briefly the gravitational escape of gases from planets and then the general nature of their atmospheres.

2. Escape of Atmospheric Gases from Planets

The history of the atmosphere of a planet and the atmosphere

retained by the planet will depend on the rates of escape of the various s from the gravitational field of the planet. The minimum velocity cape of a particle is governed by its total energy reaching a value o . The total energy is given by the sum of the kinetic energy and the gravitational potential energy. It is

$$E = \frac{1}{2} m v^2 - \frac{m M G}{R} \qquad (1)$$

where m is the mass of the particle with velocity v, and M, G, R are the mass, gravitational constant, and radius of the planet respectively. The minimum velocity which allows the particle to escape from the gravitational field is called the "escape velocity" v_e given by

$$\frac{1}{2} m v_e^2 - \frac{m M G}{R} = 0 \qquad (2)$$

or,

$$v_e = \sqrt{\frac{2MG}{R}} = (2gR)^{1/2} = 11.3 \sqrt{\frac{M_e}{R_e}} \text{ km/sec}, \qquad (3)$$

where M_e and R_e are the mass and radius of the planet in terms of the mass and radius of earth. Thus compared to the value of 11.3 km/sec on earth, for Mars with $M_e = 0.108$ and $R_e = 0.53$, the escape velocity works out to ~ 5 km/sec. Similar calculations would give 2.3, 4.3, and 61 km/sec as the escape velocities for the planets moon, mercury, and jupiter respectively. Table I gives the various planetary parameters and escape velocities.

Table I. Planetary Parameters and Escape Velocities

Name	Radius in R_o	Mass in M_o	Gravity in m/s^2	Esc. Vel. in km/s
Mercury	0.38	0.054	3.6	4.2
Venus	0.96	0.815	8.7	10.3
Earth	1.00	1.000	9.8	11.2
Mars	0.53	0.108	3.8	5.0
Jupiter	11.19	317.8	26.0	61.0
Saturn	9.47	95.2	11.2	37.0
Uranus	3.73	14.5	9.4	22.0
Neptune	3.49	17.2	15.0	25.0
Pluto	0.4	0.2	12.3	7.6

The particles can escape from only high altitudes and not only $v > v_e$ but also they must be moving outwards with low probability for collisions. The region where the probability for collisions is very much less than unity is called the exosphere. In the lower atmosphere, the distribution of particles is governed by the hydrostatic equilibrium given by

$$dP = -Pg\,dh. \tag{4}$$

Using gas law,

$$P = NkT = \rho kT/m, \tag{5}$$

one gets the differential equation for hydrostatic equilibrium as

$$\frac{dP}{P} = -\frac{dh}{H}, \tag{6}$$

where $H = kT/mg$ is the constant parameter called the scale height of the atmosphere. Thus

$$P = P_0 \exp\left[-(h-h_0)/H\right], \tag{7}$$

P_0 being the pressure at a height h_0. Similar forms of equations will be applicable for the density and the number of particles. So we have

$$\rho = \rho_0 \exp\left[-(h-h_0)/H\right], \tag{8}$$

and

$$N = N_0 \exp\left[-(h-h_0)/H\right]. \tag{9}$$

To calculate the outward flux of particles escaping the exosphere one has the flux as (considering an elementary volume)

$$F = (4\pi R_e^2) N_e \int_0^{2\pi} d\phi \int_0^{\pi/2} \sin\theta d\theta \int_{v_e}^{\infty} (v\cos\theta) f(v) v^2 dv, \tag{10}$$

where f(v) is the velocity distribution of the particles, R_e is the radius of the base of exosphere at which N_e is the atmospheric particle density. Assuming a Maxwellian distribution of velocities for the particles, the flux becomes

$$F = 2\sqrt{\pi} R_e^2 N_e \sqrt{\frac{2kT}{m}} \exp\left(-\frac{mv_e^2}{2kT}\right)\left[1 + \frac{mv_e^2}{2kT}\right]. \tag{11}$$

Using the above equation and Eq. (9), the time in which a fraction $1 - e^{-1}$ of the original content is lost by gravitational escape and only a fraction e^{-1} remains, is determined. Table II gives such "lifetimes" for the typical constituents of atmospheres in planets.

Table II. Lifetimes in Years for Planetary Atmospheric Constituents[1]

Constituent	Moon	Mars	Earth	Venus	Jupiter
H	10^{-3}	10^{2}	$10^{3.5}$	10^{3}	10^{500}
He	10^{-2}	10^{3}	10^{8}	10^{5}	10^{2000}
O	10^{1}	10^{9}	10^{35}	10^{25}	-
N_2	10^{2}	10^{17}	10^{60}	10^{40}	-
Ar	10^{9}	10^{25}	10^{80}	10^{80}	-

It must be clearly understood that the nature of the resulting equation for the lifetime is such that a small uncertainty in temperature causes a huge uncertainty in the lifetime. Probably only the exosphere temperature of earth is known within reasonable limits of uncertainty. For other planets, probably the errors are between wide limits and this should be taken into account in discussing the escape of gases from these planets. However, one can still draw some general and interesting conclusions from the foregoing discussion and the results of Table II. Except for small amounts of hydrogen probably coming from solar wind, all the terrestrial planets must have lost their hydrogen. Moon, Mars and Venus must also have lost their helium. Moon must have lost all of its atmosphere except Argon and any other heavier gas like xenon. Though not included in Table II, gases like methane and ammonia might have been dissociated by solar ultraviolet radiation and depleted by losing all the hydrogen. Hence it accounts for the scarcity

of these gases like CH_4 and NH_3 in terrestrial planets though they might have been present in the very beginning to account for the early history of the earth and evolution of living organisms. Clearly Jupiter must be retaining the constituents of its primitive atmosphere including hydrogen and hence may be expected to have CH_4, NH_3 and probably H_2O. These have been confirmed by observations. In the case of earth by a fortunate circumstance the water has been retained by the "cold trap" of the atmosphere. The temperature of the troposphere decreases with altitude very rapidly and produces the condensation of escaping water vapor to droplets that return to the ground. Also the ultraviolet light which could dissociate water and allow its hydrogen to escape is absorbed by oxygen and other constituents at high altitudes. The combination of the above circumstances has enabled the retention of water essential on our planet.

3. Basic Atmospheric Data

The basic data connected with the planetary atmospheres are the temperature, density, and composition. The major thrust of the study of planetary atmospheres is therefore the study of the above parameters. Of these, the temperature is the most important one as it is directly involved with the absorption of solar light and hence the diagnostics concerning the composition of the structure of the atmosphere. The temperature profile of the earth's atmosphere has been determined with sufficient details[2, 3] and it is shown in Fig. 1. Such a profile

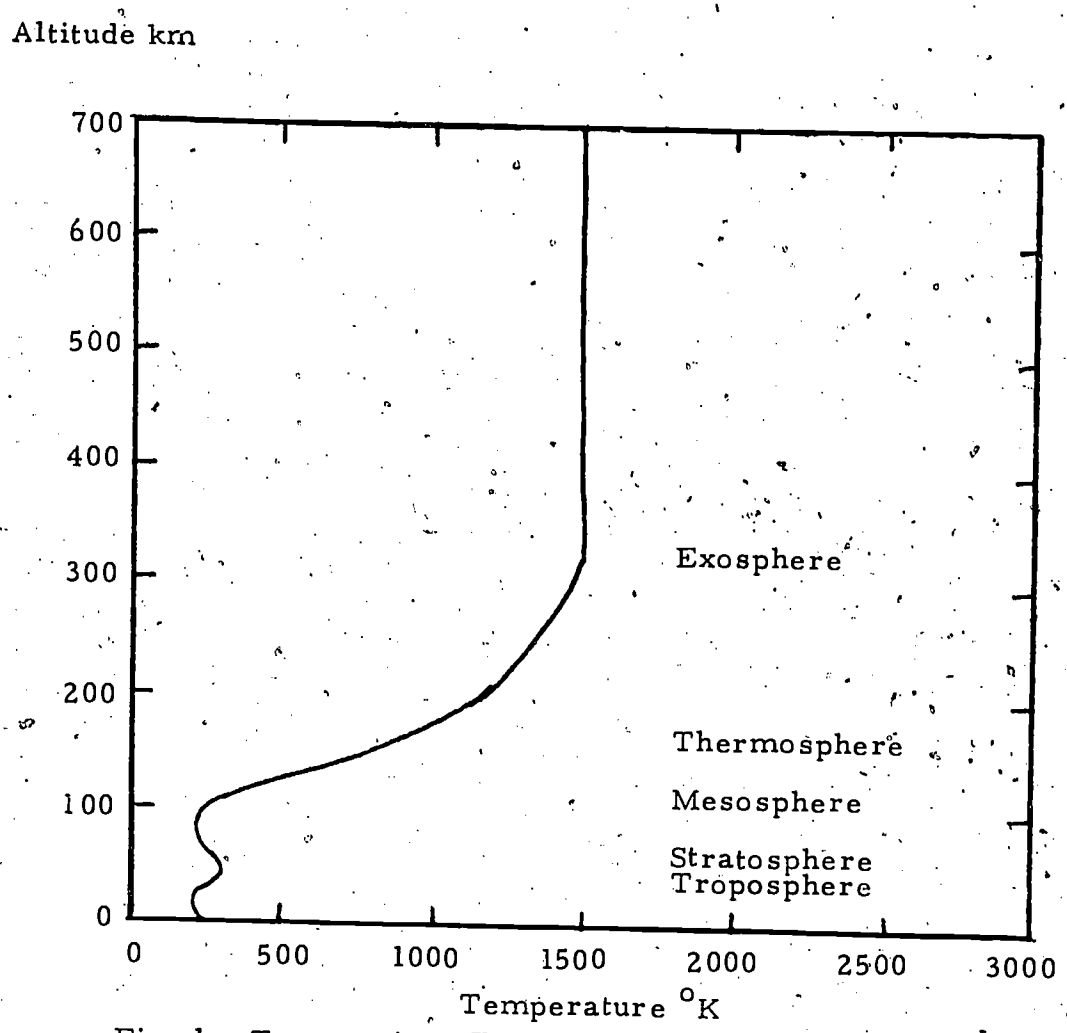

Fig. 1. Temperature Profile of Earth's Atmosphere

enables us to understand the energy transport mechanisms associated with various regions from the surface of the planet out to the inter-planetary medium.

One of the important quantities connected with our study is the "effective temperature" T_e of a planet and this can be determined using the Stefan-Boltzmann law. Let us consider the earth as an

example and if it reflects a fraction A of the incident solar radiation energy and absorbs (1 - A), for thermodynamic equilibrium (constant temperature of earth), one has

$$\pi R^2 S(1-A) = 4\pi R^2 \sigma T_e^4 \qquad (12)$$

σ is the Stefan-Boltzmann constant, R is the radius of the planet, T_e is the effective temperature and S is the solar flux at a distance of 1 A.U. (Astronomical Unit = distance between earth and sun). The value of S calculated from solar radius and temperature is nearly 1.4×10^6 erg $cm^{-2} S^{-1}$ or 2 cal cm^{-2} min^{-1}. Using a value of 0.4 for the Albedo A of earth and

$$T_e = \left[S(1-A)/4\sigma \right]^{1/4}, \qquad (13)$$

the effective temperature of earth is calculated to be $\sim 245^\circ K$. We know that the average ground temperature of earth T_g is $\sim 290^\circ K$. This increase of the temperature is due to what is called the "greenhouse effect" of our terrestrial atmosphere. Such a "greenhouse effect" must therefore be considered in the case of all planets when estimating their temperatures.

Let us discuss in general qualitative terms the importance of the above-mentioned "greenhouse effect". The fraction (1 - A) of the solar energy incident on earth is absorbed by the earth which therefore becomes heated. Such absorption is dominated by the maximum intensity of the solar radiation (which is mostly in the visible region and hence suffers

practically no attenuation by the earth's atmosphere). With the rise in temperature resulting from the absorption of the part (1 - A), the earth radiates like a black body at a temperature T_g. Most of this emission is in the infrared region ($\lambda \sim 10\mu$). Such infrared emission is strongly absorbed by the triatomic molecules like CO_2, H_2O and O_3 of the atmosphere. These molecules re-radiate this energy partly towards outer space and partly towards the earth thus providing further heatup on the surface of earth. In equilibrium

$$\sigma T_e^4 + F_d = \sigma T_g^4 \tag{14}$$

where F_d is the downward flux from triatomic molecules. To find F_d and thus T_g, one has to use the radiative transfer equations. This procedure is generally very complex. However assuming local thermodynamic equilibrium (LTE) and similar approximations, the value of T_g is given by Eddington approximation as

$$T_g = T_e \left(1 + \frac{3}{4}\tau_0\right)^{1/4}, \tag{15}$$

where τ_0 is the opacity. τ_0 for earth's atmosphere is ~ 1.9 and this value gives T_g a value of 305°K slightly higher but easily accounted for by the approximations introduced especially neglecting effects of convective transport of energy from the ground to the atmosphere. In Table III are shown the values of T_e and T_g for some of the planets.

Table III. Effective and Ground Temperatures

Planet	T_e °K	T_g °(K)	$(T_g - T_e)$ °K Greenhouse Effect
Mercury	616	616	0
Venus	235	600	365
Earth	245	305	60
Mars	209	230	21
Jupiter	105	150	45

From the above Table, one can infer in the case of mercury the absence of molecules that provide the opacity in the infrared. For venus the atmosphere is highly opaque to the infrared radiation and therefore polyatomic gases that have strong absorption bands in the IR region should be abundant. Such inferences are to be considered only for qualitative significance rather than for accurate estimates of opacity leading to other conclusions. With this foregoing discussion we will now proceed to consider the atmospheres of planets beginning with the earth's atmosphere.

4. Earth's Atmosphere

The atmosphere is divided into several layers depending on the principal property under consideration. Usually, the temperature is used as the parameter for such a division. The different layers are the troposphere, stratosphere, mesosphere, etc. The temperatures

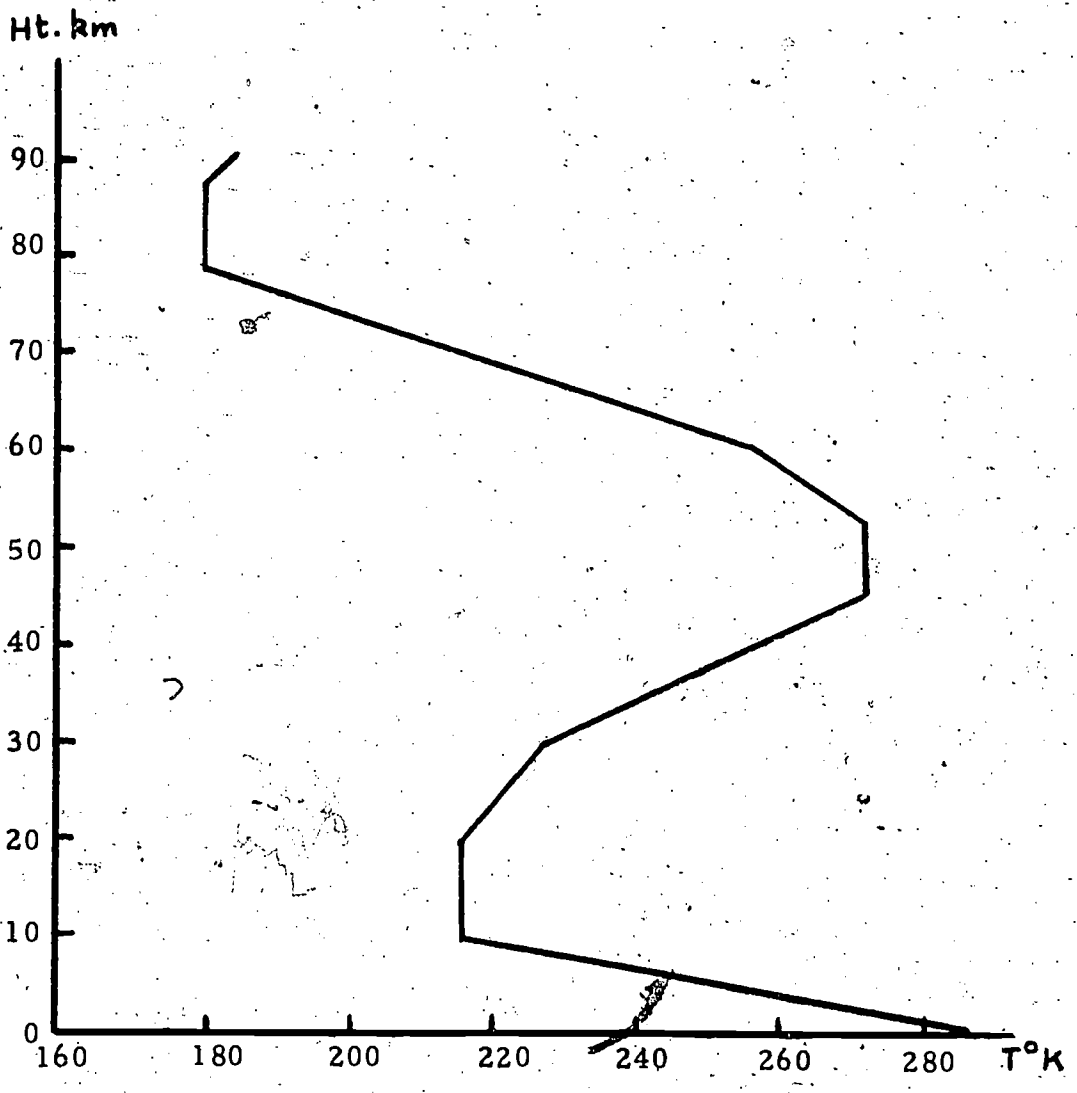

Fig. 2. Temperatures for the "Standard Atmosphere"

adopted for the various layers are shown in Fig. 2. The lowest layer troposphere extends from the ground up to ~ 13 km. The source of heat for this region is the earth's radiation and thus the temperature decreases with height. In the stratosphere, the temperature again begins to rise to ~ 290°K and the heating is due to the absorption of

ultraviolet radiation by the ozone layer which reaches a maximum concentration around 20 - 25 km. The temperature falls off with increase in height in the mesospheric layer due to the energy sink by the CO_2 and oxygen emission in the far infrared. This layer extends to ~ 90 km as may be seen from Fig. 2. Finally, the thermosphere is the region where the temperatures reach as high as 2000°K due to the far ultraviolet (100 - 2000Å) radiation from the sun. In this region photoionization and photodissociation of atmospheric constituents will take place. The thermosphere extends to an altitude of 350 ± 100 km.

While the above divisions are based on the temperatures of the various regions, the divisions in terms of the chemical composition are also of interest for our present discussion. The homosphere extending from 0 to 100 km is the region where there is total mixing of atmospheric constituents and the atmosphere has a uniform chemical composition of 28.96 mean molecular weight. The next region above 100 km and up to 1000 km, called the heterosphere is where the molecular weight decreases with altitude and the constituents are dissociation products of O_2. The layer between 1000 km and 2000 km is the heliosphere where the main constituent is helium. The region above 3000 km where the main constituent is the atomic and ionized hydrogen, is called the protonosphere.

5. Atmospheres of Other Planets

We attempt here only a brief summary of the contents of the atmos-

pheres of other planets and then discuss methods adopted to study them using spectroscopic techniques. The planet mercury, if it has any atmosphere at all, should have a very thin atmosphere probably consisting of Ar^{40} from the radioactive decay of K^{40}, Krypton, Xenon and a trace of CO_2. The atmosphere of Mars has been the subject of investigations by several workers and measurements in the 8700 Å region as well as the Mariner experiments have clearly identified the atmosphere to be predominantly CO_2. The Mariner experiments have also confirmed the presence of traces of oxygen, hydrogen, and carbon monoxide. Argon is another constituent present in large amounts.

The study of the atmosphere of the planet Venus involved the terrestrial observations in the radio, visible, and infrared regions of the spectrum and more importantly the "in situ" measurements by the instrument packages "soft-landed" on the planet. These observations have established the atmosphere of Venus to be mostly CO_2 ($\sim$ 95%) and perhaps nitrogen (3 - 4%). The strong "greenhouse effect" of CO_2 is responsible for the very high temperature on the surface of Venus as measured by the above-mentioned experiments. The heavy CO_2 atmosphere will provide the required infrared opacity.

Jupiter with its high gravity and low temperatures has been able to retain most of its original atmosphere since the gravitational escape of gases is extremely slow. Thus the Jovian atmosphere contains large amounts of hydrogen and helium. In addition, spectroscopic methods

have confirmed the presence of appreciable amounts of NH_3 and CH_4. The planets Saturn, Uranus, and Neptune are also massive ones like Jupiter and have high values for the escape velocities (see Table I). Thus their atmospheres also contain vast amounts of hydrogen and helium and also ammonia and methane. With this general summary let us consider the spectroscopy of planetary atmospheres.

6. Spectroscopic Studies of Planetary Atmospheres

In this section we will summarize briefly the general nature of the information that has been obtained on planetary atmospheres using spectroscopic techniques.[4] Major advances have been made in our knowledge of the planetary atmospheres both from ground-based observations and observations above the atmosphere through the use of various space missions. First of all, the albedo of the planet (the fraction of solar light reflected by the planet) is a primary indication of the existence of an atmosphere. A high albedo suggests a dense atmosphere due to the multiple scattering of light. Table IV gives the albedo values for some of the planets. One should also remember that icy surfaces also may show a high albedo. It is possible to infer the distribution of absorbing and scattering constituents from observations at various wavelengths.

Let us illustrate the extreme usefulness of spectroscopic methods and the possibility of getting the most valuable information about the planetary atmospheres from quantitative spectroscopy. With the

Table IV. Albedo Values for Planets

Planet	Albedo	Planet	Albedo
Mercury	0.06	Jupiter	0.50
Venus	0.75	Saturn	0.50
Earth	0.40	Uranus	0.50
Mars	0.15	Neptune	0.50

various missions in our space program and the supplementary laboratory studies as well as other ground-based observations, high resolution spectroscopy has been one of the most productive areas for major advances in our knowledge of planetary atmospheres and for postulating atmospheric models. The rotation-vibration spectra of the molecular constituents of the atmospheres of the planets and particularly the precise values of the positions as well as the intensities of the spectral lines have not only aided in the identification of the molecules present but also enabled the derivation of such properties as their temperature, pressure, and abundance. Fox[5] has summarized the species of molecules identified in planetary atmospheres with references for recent studies of their high resolution spectra. Table V gives a partial summary. For minor constituents see Fox[5].

Let us first consider the example of Venus. Besides using the positions of CO_2 lines to establish the existence of CO_2 as the main constituent of its atmosphere, the intensities of the rotational lines are

Table V. Molecules in Planetary Atmospheres

Planet	Molecule	Amount ((m-atm)
Venus	CO_2	3300
	CO	0.15
	HCl	0.002
Earth	N_2	6240
	O_2	1670
	H_2O	8 - 200
	CO_2	2 - 3
	CH_4	0.01 - 0.02
	H_2	0.004
	CO	0.0005 - 0.008
Mars	CO_2	54 - 90
	H_2O	0.01 - 0.04
	CO	0.05 - 0.2
Jupiter	H_2	67000 - 85000
	CH_4	30 - 100
	NH_3	13
Saturn	H_2	190000
	CH_4	40 - 350
Uranus	H_2	250000 - 480000
	CH_4	3500
Neptune	H_2	250000 - 480000
	CH_4	6000

used to estimate the "rotational temperatures" of the gas. For a clear atmosphere, the line width W is related to the rotational quantum number J and "rotational temperature" θ_r as[6]

$$\log_{10} \frac{W}{2J+1} = \text{Const.} - \frac{0.244\, J(J+1)}{\theta_r} \qquad (16)$$

For a scattering atmosphere,[7] the corresponding relation is

$$\log_{10} \frac{W(J)}{\sqrt{2J+1}} = C - \frac{0.122\, J(J+1)}{\theta_r} \qquad (17)$$

Young et al.,[8] obtained an average rotational temperature of 244°K assuming a square-root absorption law. Further, Young[9] also studied the effective pressure for the line formation and concluded that the weak absorption lines are indeed formed deeper in the atmosphere. In the case of Mars, a series of spectroscopic studies[5] have been made using the bands at 0.87, 1.05, 1.6 and 2.0 μ and abundances as well as surface pressures have been deduced. A rotational temperature of $\sim$ 205°K has been determined.

Jupiter, the largest planet in the solar system, has an atmosphere whose composition, structure, and dynamics are complicated. Owen[10] has reviewed the spectral studies of the Jovian atmosphere and emphasized that a careful study of Jupiter could reveal the "essential clues to the origin and evolution of the solar system, and perhaps life as well". Let us first discuss briefly the most abundant species (namely hydrogen) in the atmosphere of Jupiter and other massive planets like Saturn, Uranus, and Neptune.

Hydrogen in its molecular form has no spectrum allowed by the selection rules for dipole radiation. Thus, following the suggestion of Herzberg[11], the focus was on the quadrupole rotation-vibration spectrum. Several lines belonging to this spectrum were identified in the laboratory

and then compared with the spectrum of Jupiter. With precise measurements of intensities in laboratory studies, it was possible to obtain estimates of the abundance of hydrogen at about 85 ± 15 km-atm. An effective temperature of 145 ± 20°K was also deduced. The positions of the quadrupole rotation-vibration lines that have been measured are summarized by Fox.[5]

The importance of high-resolution spectroscopic investigations is best illustrated by its use in determining the rotational temperature and abundance using the equivalent widths of the lines in the $3\nu_3$ band of CH_4 molecule present in the atmosphere of Jupiter. The band is centered at about 9050 cm^{-1}. In the determination of the rotational temperature the line positions and relative intensities were taken from high-resolution laboratory spectra. An abundance of $\sim$ 30 m-atm was deduced for methane in Jupiter. The most significant result is that accurate values of CH_4 abundance and H_2 would provide the C/H ratio which is very relevant to the origin and evolution of the solar system. Also the red band at 6450 Å due to NH_3 has been extensively studied and an effective pressure of $\sim$ 2.5 atm was deduced. Other molecules have also been identified to be present in small amounts and this was done using the laboratory and planetary spectra in the photographic infrared region. Using methane spectra, the planets Saturn, Uranus, and Neptune have been found to have CH_4 as one of their atmospheric constituents.

The above discussion has been kept very general and brief consistent with the aim of this introduction to planetary atmospheres. A detailed study of spectroscopic methods of investigating planetary atmospheres will present an interesting topic by itself especially the comparisons of high-resolution laboratory data. With the planned Large Space Telescope (LST) program and the highly sophisticated infrared and ultraviolet as well as visible spectrometers that have been developed for this program during the last few years, the study of planetary atmospheres is entering a new and exciting era. There is definite hope in the near future to understand more fully the evolution of our solar system and the predictions for the future behavior of its components.

REFERENCES

1. M.D. Papagiannis, Space Physics and Space Astronomy, Gordon and Breach, Science Publishers, New York, N.Y (1972).

2. C. Sagan and W.W. Kellog, Annual Reviews of Astronomy and Astrophysics 1, 235 (1963).

3. S.I. Rasod, AIAA Journal 1, 6 (1963); Also in "Origin of Life" (Ed. C. Ponnamperma) American Elsevier, New York (1971).

4. A.E.S. Green and R.J. Wyatt, Atomic and Space Physics, Addison-Wesley Publishing Co. Inc., Reading, Massachusetts (1965), p. 474-481.

5. K. Fox in Modern Research in Molecular Spectroscopy, Ed. K.N. Rao, Academic Press Inc., New York, N.Y. (1973) pp 79-114.

6. H. Spinrad, Publ. Ast. Soc. Pacific 74, 187, 62 (1962).

7. J.W. Chamberlain and G.P. Kuiper, Astrophys. J. 124, 399 (1956).

8. L.D.G. Young, R.A. Schorn, and E.S. Barker, Icarus 13, 58 (1970).

9. L.D.G. Young, Icarus 13, 449 (1970).

10. T. Owen, Science 167, 1675 (1970).

11. G. Herzberg, Astrophys. J. 87, 438 (1938).

X-RAY ASTRONOMY

1. Introduction

Photons with energies in the range 100 eV to 200 keV would describe the energies in X-ray astronomical studies. Due to the very strong absorption by the earth's atmosphere of photons in the above range, the experiments in X-ray astronomy have to be necessarily carried out with X-ray detectors above the earth's atmosphere using rockets, balloons, and satellites. Historically, the studies in X-ray astronomy began with the first direct observation of solar X-rays in 1948 and continued during the 1950's with many interesting results. Although till 1962 the sun was assumed to be the only source, in addition to the solar X-rays, other X-ray sources like the supernovae, the Crab nebula, and magnetic stars deserve special mention as these have been identified since the experiments of Giacconi, et al.[1]. In this module, we will discuss mainly the techniques that are used in the studies of X-ray astronomy, the instruments that have been developed, and some of the interesting results that have been obtained recently.

There are several reasons for pursuing this important branch of astrophysics. In the first place, it will enable us to understand new and unexpected phenomena that in turn will influence our ideas about the universe. Secondly, it is very important and interesting to examine the physical condition within these X-ray sources and the

information about the generation of X-rays within the sources by observing the X-ray fluxes. Thirdly, from a study of the absorption of low energy X-rays by the interstellar medium, it is possible to obtain the density of interstellar gases. In this connection, the problem of the concentration of molecular hydrogen in interstellar medium deserves also a special mention. Since the optical and radio observations have not yielded much information about intergalactic gas, the fourth reason for studying X-ray fluxes from intergalactic gas is the great cosmological significance that such studies provide in detecting "missing matter".

2. Observational Techniques.

In X-ray astronomy, as in other branches of astronomical observations, the quantities that are relevant are the intensity, the wavelengths present, and the polarization characteristics. The general requirements for a successful experiment should include a detector, collimator, and an analyzer. However, there is a basic difference between these experiments and others. Since there is a very strong absorption of the X-rays by the earth's atmosphere, the instruments must be carried by rockets or satellites beyond the earth's atmosphere and measurements should be made from those altitudes. Naturally this aspect of experiments may impose certain limitations on the type of experiments besides limitations on the weight and volume of the instrument package to be carried by rockets or satellites. Also, the rocket or satellite carrier has to

be oriented towards the possible source and stabilized in that position with the help of some suitable attitude control mechanism. For very low fluxes of radiation that are present, one needs highly efficient quantum detectors in the instrument packages.

The instrumentation that has been developed so far in the field of X-ray astronomy is in no way comparable to the sophistication attained for use in the optical and radio regions of the spectrum. The techniques that are to be used here should (i) detect the location, size, shape, and extent of the source, (ii) measure the total intensity of the source in the X-ray region, (iii) examine the variation of intensity with time, (iv) polarization of the radiation, and (v) structure of emission lines and absorption edges. Only such detailed studies would enable us to obtain the maximum amount of information about these X-ray sources. Let us therefore consider the various techniques that have been used in these studies.

In developing experimental techniques in the field of X-ray astronomy, significant contributions have been made by three groups viz., (i) American Science and Engineering-Massachusetts Institute of Technology (ASE-MIT) group; (ii) Naval Research Laboratory (NRL) group; and (iii) the Lockheed group. The healthy competition between these various groups has been primarily responsible for the rapid development of instrumentation for observation of even very weak sources. The first experiment by ASE-MIT group led by Giacconi, et al., in 1962 employed a set of large geiger counters to study X-rays

from scattering of the solar radiation by the moon. The counters, carried in an Aerobee rocket, were sensitive to the wavelength region 2 to 8 Å and each had a window area of 20 cm^2 with mica windows of varying thicknesses. The strong spatial anisotropy indicated a strong extra-terrestrial source of X-rays. The source was detected close to the center of the galaxy and named Sco XR-1 because of its location in the constellation of Scorpius. This experiment was followed by another from NRL group with a counter of sensitivity 10 times greater than the previous one and confirmed the source.

The basic experimental set-up should consist of a collimator which transmits X-rays coming from the source within a certain range of angles, a detector that can receive the incident X-rays and measure its flux in terms of the effects produced, and an analyzer which can be used to study the wavelength as well as polarization characteristics of the X-rays received. Let us therefore look at each of these three stages and discuss the basic instrumentation for observations.[2, 3]

(a) Collimators

For identifying the locations and angular sizes of the X-ray sources, it is necessary to limit the field of view of the detectors using suitable collimators. In one type of collimators, called the Cellular Collimators, one can study fields of view of different shapes and different angular widths. The collimator is made in the

form of a honeycomb of long metal cylinders limiting the field of view within 1°. With these it is possible to scan only a small area of the sky.

Another type of collimator (called "modulation collimator") with high resolution and wide field of view has been developed by the ASE-MIT group. The design involves two grids of parallel wires separated by a small distance and mounted in front of the window of the detector as shown in Fig. 1.

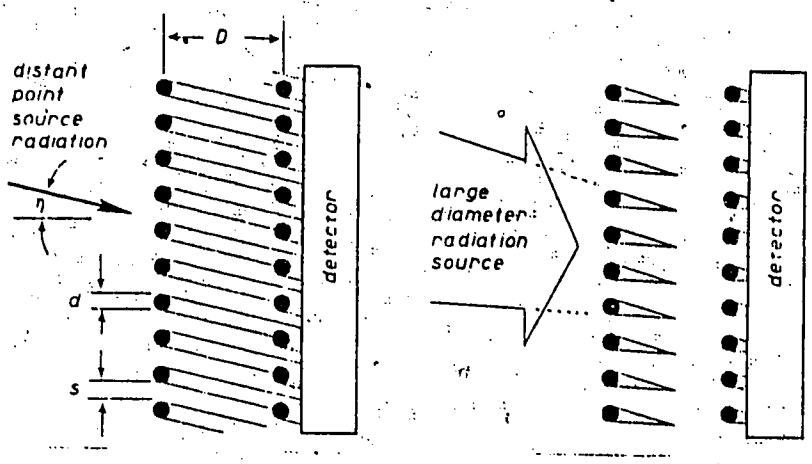

Fig. 1 Configuration of a Modulation Collimator

The wires are of the same thickness as the spacing between the wires. For a parallel beam of incident X-rays if the shadow cast by the first grid falls on the wires in the second grid there will be

maximum transmission. Such configurations will be possible for a number of angles. This type of collimator has the decided advantage of very high resolution and the feasibility to scan a large area of the sky. If the diameter of the wires (equal to the spacing between the wires) is d and the inner grid is at a distance D from the outer grid, the angular distance between maxima will be d/D. This therefore will enable the size of the source to be determined and angular resolution of one minute of arc is possible with this arrangement.

To improve the resolution further and provide unambiguous results with several sources in the field of view or study an extended source, an image-forming telescope is used. These telescopes depend on the total external reflection of X-rays under grazing incidence and use two reflecting surfaces, a paraboloid and a hyperboloid as shown in Fig. 2. Such instruments which make use of efficient scattering of X-rays at grazing incidence are the most useful ones in X-ray detection techniques. An optical sensor indicates the position of the detector relative to a known source like the sun or moon or a bright star.

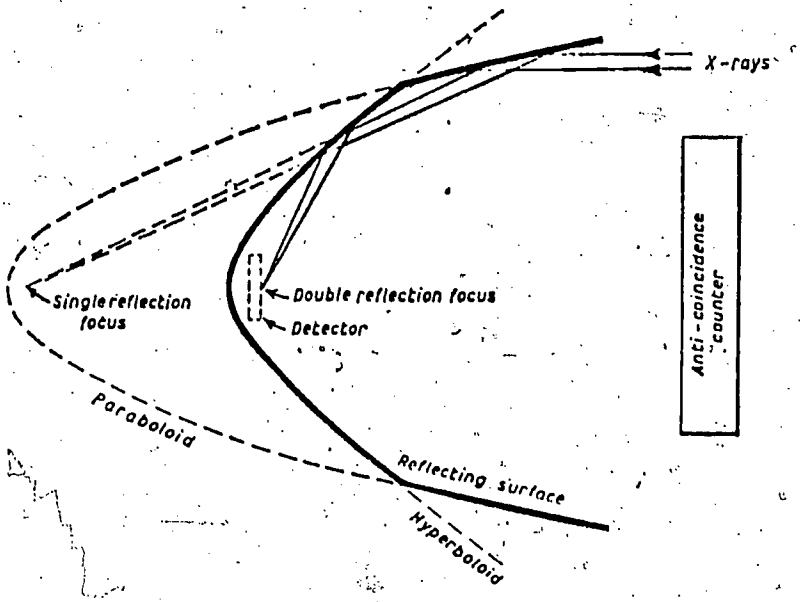

Fig. 2 Principle of a Reflecting X-ray Telescope

(b) Detectors

Due to the low photon fluxes and the particular needs, the detectors to be used in studying X-rays should have a sensitive area of 10 to 1000 cm^2 and have high efficiency as well as well-defined energy response. There are three different types of detectors commonly used for experiments in X-ray astronomy. They are: (i) Proportional Counters (gas counters like Geiger counters; (ii) Scintillation Counters, and (iii) Photoelectric Devices.

The Proportional Counters are gas counters filled with a gas at suitable pressure and depend on the ejection of the photoelectrons from the gas and the formation of electron-ion pairs as a result of the ionization by the incident X-ray energy. The efficiency of such

a counter is given by

$$\varepsilon(\lambda) = e^{-\mu_w t_w}\left(1 - e^{-\mu_g t_g}\right) \qquad (1)$$

where μ_w, t_w are the absorption coefficient and thickness of the window material, and μ_g, t_g are the corresponding quantities for the gas in the reservoir. The limiting values of the thickness of the window will depend on μ_w and the pressure of the gas inside. Normally, the lower limit of X-ray photon energy is 1 keV although this has been pushed to lower values (~0, 4 keV) using special windows. The upper limit of energy is determined by the transparency of the gas in the counter. A schematic layout of a gas proportional counter is shown in Fig. 3.

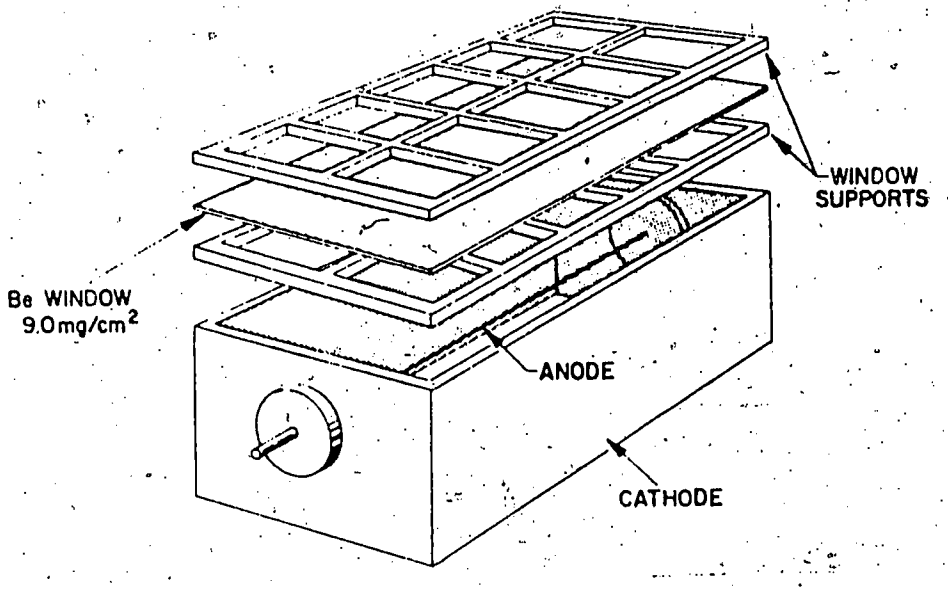

Fig. 3 Schematic Layout of a Thin Window Gas Proportional Counter

For example, with xenon gas in the counter, up to 50 keV energies of the incident photons can be detected. The noble gas is

preferred since no energy loss will take place as in the case of polyatomic molecules where energy may be dissipated in exciting the gas to its rotational or vibrational states. While a pure noble gas counter is very unstable, the addition of a polyatomic quench gas (like CH_4, CO_2, etc.) will enable absorption of the ultraviolet light from the noble gas. Proportional counters use thin windows of an organic material like mylar or teflon coated with a thin metal layer to eliminate the sensitivity to ultraviolet light and also to reduce the gas leakage. However, it is clear that the efficiency of the counter will depend on the X-ray photon not being absorbed by the window material but absorbed by the gas in the counter. Beryllium and metal-coated mylar have been used with considerable success. The output pulse is proportional to the number of ions produced which in turn depends on the incident X-ray energy.

The scintillation counters use the photoelectron emitted from the collision of the incident X-ray photon with the scintillation material. The light photons emitted before the capture of the electrons will be a measure of the electron energy and hence of the incident X-ray photon. The light photons are detected by a photomultiplier. Generally, the scintillation detectors are used for photon energies greater than 10 keV. These counters are more efficient than a gas counter and have higher energy resolution as shown by several rocket experiments. NaI has been used in scintillation counters to

observe X-rays from Crab Nebula from a balloon and from Sco XR-1 from a rocket as well as from Cygnus sources. CsI has also been used as a very useful scintillating material. While NaI gives more light and thus better energy resolution, it is somewhat difficult to handle due to its hygroscopic nature.

Photoelectric detectors without scintillation crystals were designed since the discovery of the very high efficiency of some alkali halide for photoelectron emission. No windows need be used and this coupled with high efficiency at long wavelengths would make these detectors ideally suited for studies at low energies. The photoelectrons from the alkali halides are electrostatically focussed on the first dynode as in an ordinary photomultiplier. Sensitive areas of nearly 40 cm^2 have been used and their efficiency range from 8% for 5 keV photons to $\sim$25% for 0.8 keV photons. The photoelectric detectors also need filters for absorbing the ultraviolet light.

It must be mentioned that in the use of the above-mentioned detectors which are not just unique to detect X-rays, it is essential to reject the diffuse background like those due to the primary cosmic radiation or other charged particles. Such rejection is easily achieved by the configurations and combinations of detectors. For example, two scintillation counters may be arranged with different scintillation materials such that one will respond to the photons that are incident while the other rejects charged particles. In photoelectric devices a

thin window may be employed to shut out visible and ultraviolet light without reducing the sensitivity of the detector to incident X-ray energy.

3. Mechanisms for Cosmic X-ray Emission

In this section we are concerned with the various mechanisms for the production of X-rays in a cosmic setting and we will examine the physics of the various processes with definite formulae important for applications. There are three definite processes for the production of X-rays that need to be discussed. These are: (i) Magnetic Bremsstrahlung (or Synchrotron emission), (ii) Bremsstrahlung radiation by electrons in the Coulomb field of a nucleus and (iii) Inverse Compton Effect.

(i) Magnetic Bremsstrahlung (Synchrotron Radiation)

Consider a particle of charge e and velocity $c\beta$ ($\beta = \frac{v}{c}$) experiencing an acceleration $\underline{a}$. To calculate the energy radiated by such an accelerated charge one can use classical electrodynamics and recall the Larmor radiation formula. Using the expressions for the electric (E) and magnetic (B) fields, one has the instantaneous energy flux given by the Poynting vector

$$S = \frac{c}{4\pi} \underline{E} \times \underline{B} \qquad (2)$$

and

$$\underline{B} = \underline{n} \times \underline{E} \qquad (3)$$

$\underline{n}$ being the unit vector. The power radiated to infinity per unit

solid angle then becomes

$$\frac{dP}{d\Omega} = \frac{e^2}{4\pi c^3} a^2 \sin^2\theta \tag{4}$$

where θ is the angle between the vectors $\underline{a}$ and $\underline{n}$. Integrating over all solid angles, the total instantaneous power is

$$P = \frac{2}{3} \frac{e^2 a^2}{c^3} \tag{5}$$

which is the Larmor radiation formula.

To use the above expression for the relativistic electrons with energy $E = \gamma mc^2$ in a uniform magnetic field $\underline{B}$, we can generalize the above results. $\gamma = 1/\sqrt{1-\beta^2}$. A relativistic particle spirals in a magnetic field as shown in Fig. 4 with the relativistic narrowing of the beam within a small angle as shown.

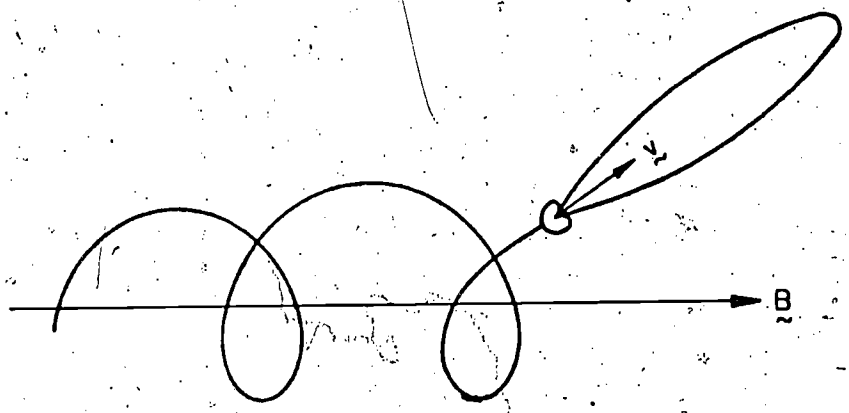

Fig. 4 Relativistic Particle Spiraling in a Magnetic Field $\underline{B}$

The equation of motion is given by

$$\frac{d}{dt}(\gamma mc\beta) = e\,\underline{\beta} \times \underline{B} \tag{6}$$

and the particle experiences an acceleration perpendicular to its velocity. The particle radiates as though it were spiraling in a

magnetic field

$$B_T = \gamma \cdot m c^2 \beta / e r_c \tag{7}$$

To calculate the power one has to use

$$a = e \gamma \beta_\perp B \tag{8}$$

where $c\beta_\perp$ is the velocity component perpendicular to the field.

The total power radiated is thus

$$P = \frac{2}{3} r_0^2 c \gamma^2 B^2 \beta_\perp^2 = 1.6 \times 10^{-15} \gamma^2 B^2 \beta^2 \sin^2 \alpha \quad \text{ergs/sec} \tag{9}$$

where $r_0 = e^2/mc^2 = 2.82 \times 10^{-13}$ cm for an electron and α is the pitch angle between β and B. For isotropic distribution of particle velocities the mean radiated power is

$$P = \frac{4}{9} r_0^2 c \gamma^2 B^2 \beta^2 = 1.1 \times 10^{-15} \gamma^2 B^2 \beta^2 \quad \text{ergs/sec} \tag{10}$$

Since P is the rate of emission of energy, one can talk about the "half life" in which time the energy $\mathcal{E}(t)$ of the electron will be reduced to one half of its initial value ($\mathcal{E}_0$). Using the relation

$$\mathcal{E}(t) = \mathcal{E}_0 / (1 + \beta \mathcal{E}_0 t) \tag{11}$$

the "half life" can be calculated by setting $\mathcal{E}(t) = \mathcal{E}_0/2$.

The magnetic Bremsstrahlung model has been used very successfully to explain the origins of X-rays from Tau XR-1 and Cyg XR-1. The most important consequence of this model is the presence of large numbers of ultrarelativistic electrons in the Crab nebula and similar sources. For example, with magnetic field B

nearly 10^{-3} to 10^{-4} Gauss and $\mathcal{E}_o$ - 40 keV, the "half-life" for the electrons works out to be $1.6 \times 10^{+7}$ secs to 5.1×10^{8} secs or 0.5 to 15 years. When we realize the fact that the Crab is more then 900 years old, it can be seen that it is an active source with a steady supply of relativistic particles and not just a slowly decaying aftermath of a stellar explosion. The origin of these relativistic electrons is perhaps the decay of the charged mesons produced in proton-proton collisions. For proper identification of the magnetic Bremsstrahlung model with any of the X-ray sources, the validity has to be established from X-ray polarization measurements. However, polarization of weak fluxes is somewhat difficult to measure.

(ii) Bremsstrahlung mechanism refers to the creation of photons as a result of the collisions of relativistic electrons with atomic nuclei as well as electrons in the medium. The X-ray emission from a hot optically thin nonrelativistic gas or from hot electrons in a cold plasma can be explained by the thermal Bremsstrahlung mechanism. The emission of high energy photons is as a result of Coulomb scattering which causes the electrons to accelerate and thus radiate energy. The former process of X-radiation from a hot gas found in the envelope around a Supernova or in the envelope of a radiogalaxy or a star is more important. Hence we will discuss briefly this mechanism. Such a study is also

of interest in thermonuclear research.

The collision of an electron with an atomic nucleus is shown in Fig. 5.

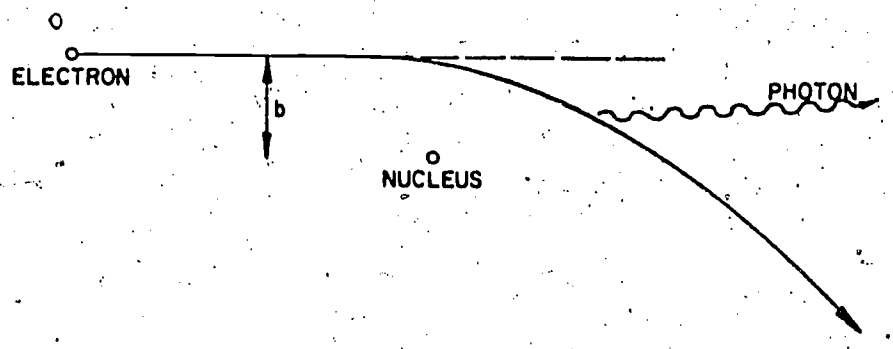

Fig. 5 Bremsstrahlung Emission from Collision of Electron with Nucleus

The power radiated by the electron accelerated in the Coulomb field of the nucleus of charge Ze is given by Larmor's formula as

$$P = 2e^2a^2/3c^3 \tag{12}$$

Since most of this energy is radiated near the distance of closest approach

$$a \simeq Ze^2/mb^2 \tag{13}$$

For the effective collision time which is nearly b/v, the total energy radiated is

$$\Delta W(b) \simeq \frac{2}{3}\frac{Z^2e^2}{c^3}\left(\frac{e}{mb^2}\right)\frac{b}{v} \tag{14}$$

The power radiated by an electron flux of $N_e v$ is

$$\frac{dP}{dv} \simeq 2\pi N_e N_z v \int \Delta W(b)\, b\, db = \frac{4\pi}{3}\frac{e^6}{m^2c^3 b_{min}} N_e N_z Z^2 \tag{15}$$

where N_z is the ion density and b_{min} is the minimum impact parameter and equals $\sim \hbar / mv$. Rewriting in terms of W the energy of the incident electron,

$$\frac{dP}{dv} \simeq \frac{8\pi}{3} Z^2 \alpha^3 \lambda_e^2 W v N_e N_z \qquad (16)$$

where $\alpha = e^2/\hbar c = 1/137$ and $\lambda_e = h/mv$ = DeBroglie wavelength. A more exact calculation gives

$$\frac{dP}{dv} = \frac{16\pi}{3\sqrt{3}} Z^2 \alpha^3 \lambda_e^2 W v g_B N_e N_z \qquad (17)$$

including g_B the Bremsstrahlung Gaunt factor which is ~ 1.

The electrons for a plasma in equilibrium obey the Maxwellian distribution of velocities given by

$$f(v) = 4\pi \left(\frac{m}{2\pi kT}\right)^{3/2} v^2 e^{-mv^2/2kT} dv \qquad (18)$$

and the resulting Bremsstrahlung spectrum from a hot plasma is of the form

$$I(\nu) \propto \exp(-h\nu/kT) \qquad (19)$$

In many old novae, the above Bremsstrahlung mechanism seems to be operative. Sco XR-1 is a good example where X-ray line emission would be expected. High resolution instruments should enable us to study the many lines leading to a fuller understanding of the processes taking place in such sources. However, it must be noted that many old novae resembling Sco XR-1 are not X-ray sources but are often surrounded by a halo of hot gas giving rise to optical Bremsstrahlung. Another possibility is to explain the spectrum of

the supernovae remnant group in terms of the X-ray emission coming from a hot dilute gas plasma surrounding the hot decaying nucleus. The heat is supplied by the radioactive decay of the heavy elements produced in a supernova explosion.

(iii) Compton scattering is a third possible mechanism whereby X-rays may be produced as a result of a high energy electron giving some of its kinetic energy to a low energy photon. For an electron with an initial energy $\gamma m_e c^2$ where $\gamma >> 1$ after a collision with a low energy photon of energy $\mathcal{E}$, it can be shown that the energy of the scattered photon is

$$\mathcal{E}_c \simeq \gamma^2 \mathcal{E} >> \mathcal{E}. \qquad (20)$$

The scattering in such cases is really the inverse Compton scattering and in contrast to the usual degradation of photon energy, this is a photon enhancement process.

In astrophysical situations, photon densities are relatively high, electron densities are low, and the energy spectrum of cosmic electrons obeys a power law up to $10^{11} - 10^{12}$ eV. As shown in Figs. 6 and 7 below, the scattering processes in the lab frame (s) and in the rest-frame of the electron (S') can lead to equations for the scattered energies of the photon and the electron.

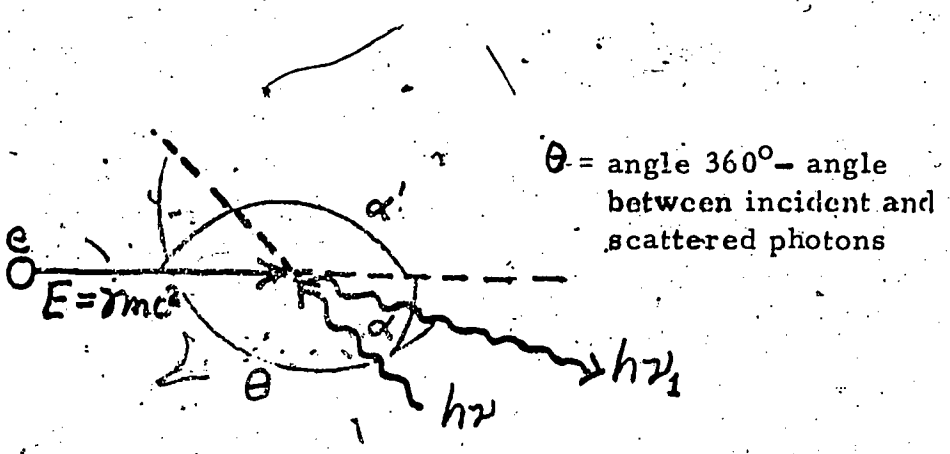

Fig. 6 Lab Frame -Compton Scattering

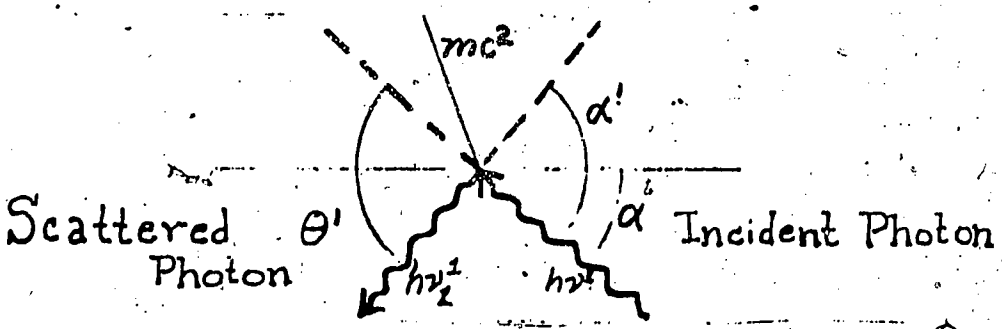

Fig. 7 Rest Frame of the Electron - Compton Scattering

For a more detailed discussion of the mechanisms and the results refer to the summary on recent developments.[4]

4. Results of Observations from X-ray Sources

As was mentioned earlier the observations in X-ray astronomy have to be carried out from rockets or bailoons or satellites. The early studies were made with rockets and necessarily these experiments were at a considerable disadvantage because of the extremely short times available to scan the sky. Of course in spite of this tremendous progress has been made since 1962 in identifying X-ray sources and to date more than 160 sources have

been observed. For many of these detailed studies have been made and models of X-ray emission mechanisms have been postulated. Needless to add that the models are in continuous debate and refinement as a result of more experimental evidence being accumulated every day.

The first and strongest discrete X-ray source discovered is Sco XR-1 using an Aerobee rocket at an altitude 80 km for a duration of 350 secs. The location of Sco XR-1 was determined to an accuracy of about 10^{o} and quite close to the galactic equator. Following Sco XR-1 discovery, with more sophisticated detectors the sources Cyg XR-1 and Tau XR-1 were also detected. The latter though a weak source in Taurus was of much interest as the Crab nebula also lay in that region of the sky. With improved detection techniques, by 1963 the existence of Sco XR-1 had been confirmed eight times and its position located to within 1^{o}. Besides confirmation of the Taurus source the intensity of the weak source was found to be 1/8 of that of Sco XR-1.

The following phase of development of X-ray astronomy consisted of improving the sensitivity of the detectors to find new sources which were too weak to be observed in the first series of experiments, improving the accuracy in fixing the position of the source by refining detector techniques, and the study of the energy spectrum of the stronger sources in order to fit the models. Thus, in general the studies have proceeded along two principal directions: (i) to fix

the celestial coordinates of the sources and (ii) to measure carefully the spectrum in detail including polarization characteristics and variability.

In the early stages, the sources were all thought to lay in the galaxy and were probably remnants of supernovae. With the exception of Sco XR-1 (which is only 20^{o} from the galactic equator), ten of the first observed sources were grouped along the galactic plane. The rocket experiments of the NRL group (Bryam et al., [5]) produced some very interesting results that changed the earlier belief that most sources were in the galactic plane. NRL experiments used two large Geiger counters of total area 450 cm^2 and a honeycomb collimator (defining a field of view of 8^{o}). Not only the overall sensitivity of the instrument was increased by a factor of four (with angular resolution of 1.5^{o}) but also the rocket carrying the instrument payload was made to spin slowly at 4 revolutions per minute. The experiments established to existence of extra-galactic sources for the first time and these were confirmed by subsequent experiments of NASA. The most important result of NRL experiments was also the variability of the sources in the Cygnus region and these had proved to have far reaching implications. In addition to sources Vir XR-1 and Leo XR-1 with balloon borne instruments Cyg XR-1 and other groups of sources in the region of the Coma cluster of galaxies have been identified.

Fig. 8 shows the principal X-ray sources and many of them lie within $\pm$ 15° of the galactic plane. Some of them could be related to the supernovae remnants. Friedman et al.,[6] of NRL had arranged the sources known up to that time into one group lying in the Cygnus-Cassiopeia region within $\pm$ 7° of the galactic equator and another

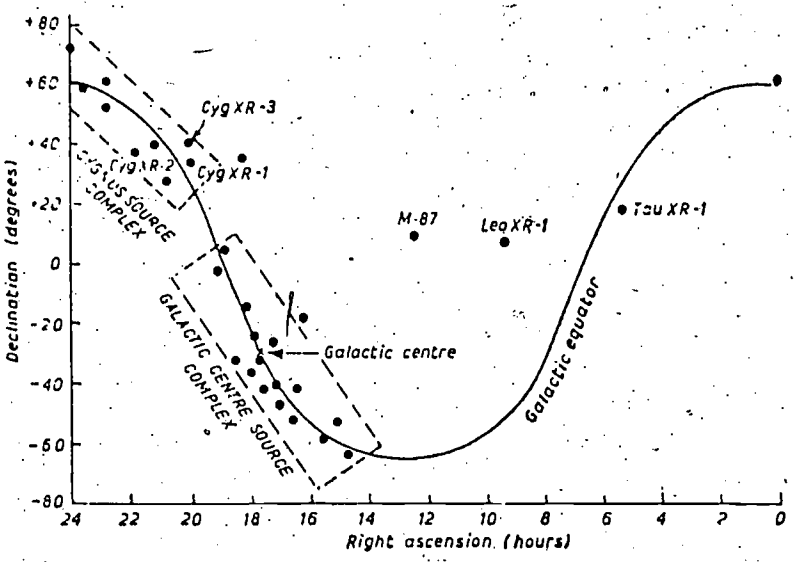

Fig. 8 Map Showing Some Principal X-ray Sources

group lying within $\pm$ 3.5° of the galactic equator in general direction of the center of the galaxy. These can be associated with the position of the spiral arms of the galaxy. For a detailed account of the nature of the spectra of these sources, the reader is referred to the joint discussions on X-ray astronomy with reports from Giacconi and others.[7]

Since 1963 one of the things that had been very puzzling and therefore raised more questions is the variability of the X-ray sources. Naturally the variation of intensity of a source with time makes it difficult to compare the observations of different groups or combine the results of experiments done by the same group at different times and draw meaningful conclusions. The variation in the relative intensities of Cyg XR-1 and Cyg XR-2 is a good example. At one time it was noticed that Cyg XR-1 was slightly stronger than Cyg XR-2 and then the situation reversed at a later time. The strongest and most studied sources Sco XR-1 and Tau XR-1 have not shown any strong variations. This picture has changed since the advent of satellites that can be used for observations over extended periods of time. The most notable satellite which provided the giant leap forward in the study of X-ray astronomy is the "UHURU" launched by NASA in 1970. Fig. 9 shows the nature of Uhuru instrumentation. Each collimator defines nearly 840 cm^2 effective area for X-ray detection. Energy band width is 2 - 20 keV. Fig. 9 shows the scheme of observation of the sky by Uhuru detectors. The spin axis can be commanded anywhere in the s. y with a stability of 1^o in one day.

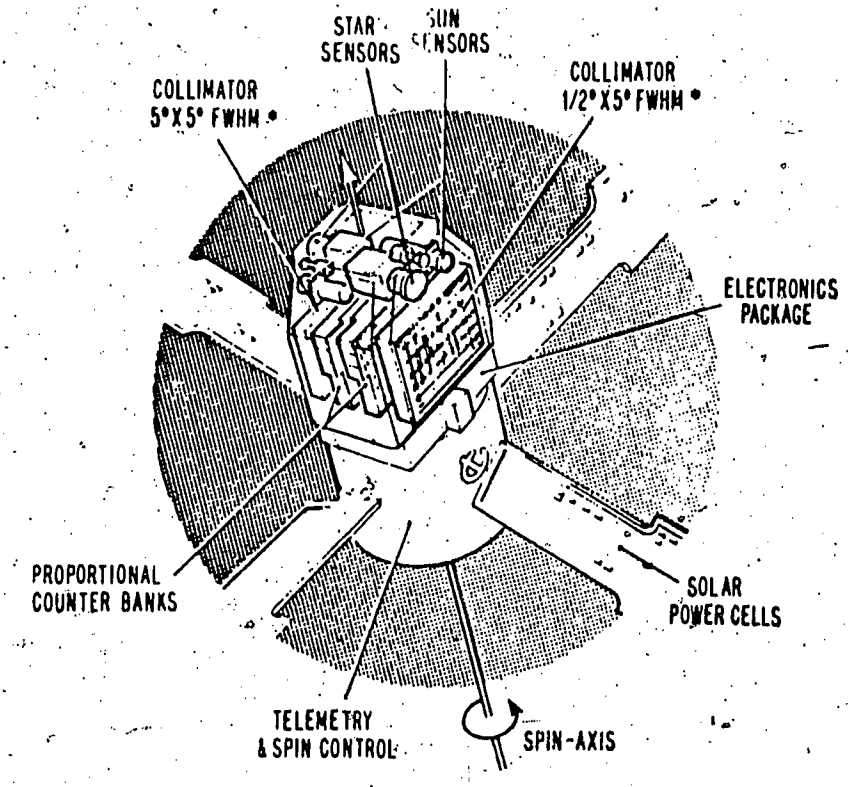

Fig. 9 Exploded View of UHURU Satellite

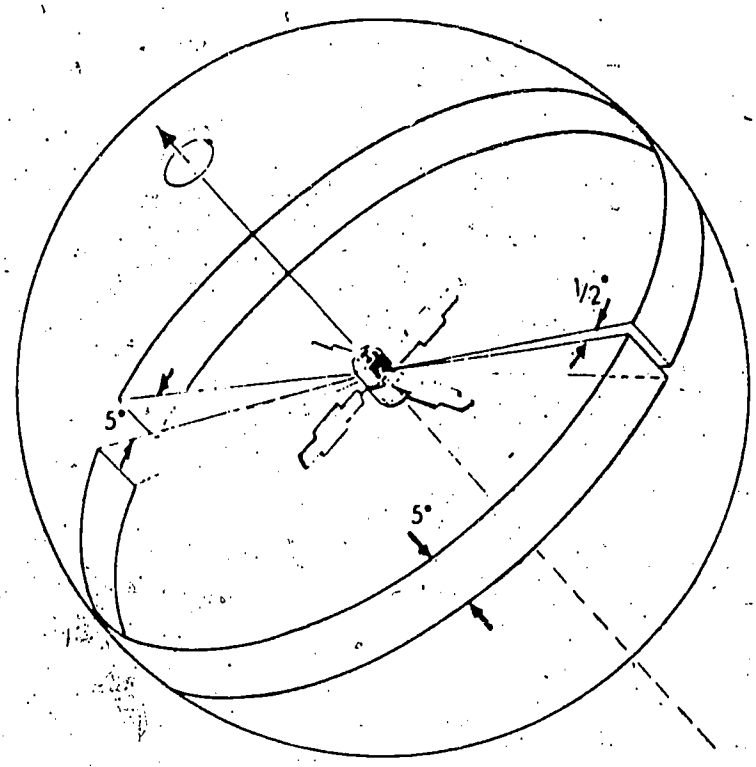

Fig. 10 Observation of Sky by Uhuru Detectors

No discussion on X-ray astronomy would be complete without the mention of the most significant results provided by the Uhuru satellite. This satellite was launched from a platform off the coast of Kenya on the seventh anniversary of that nation's independence. Uhuru (meaning "freedom" in Swahili) rotating slowly every 12 minutes high above the earth fed the data obtained by the sweep of its X-ray telescope into a control center on earth directed by Giacconi and his associates at Cambridge. Among the many significant observations by Uhuru, the most notable achievement is the proof it has provided for the existence of binary star systems and "black holes". Centaurus X-3 and Hercules X-1 are two of the sources pinpointed by the Uhuru satellite and these appear to be part of binary star systems with a neutron star as one of the partners. X-rays from Centaurus X-3 arrived precisely every 4.84239 seconds and from Hercules X-1 they arrived every 1.23782 seconds. As in the case of "black holes", the tiny neutron star would be pulling gases from its larger companion and the gases would be heated to such high temperatures as they approach the neutron star that X-rays would be emitted. Further, because of the magnetic fields surrounding the neutron star, these X-rays instead of being dispersed in all directions would be focussed into a beam. The phenomenon is similar to the neutron star as a "lighthouse" beacon. During the rotation of the neutron star the signal crosses the path of the earth

and is registered by "Uhuru" satellite.

Another most significant result of Uhuru's contributions is in connection with Cygnus XR-1 and the evidence for the existence of a "black hole". After the Uhuru satellite pinpointed the source in the constellation Cygnus, the radio astronomers got a definite fix from its radio emissions. Then the optical astronomers found the existence of a huge star, a "class 3 super-giant giant" with a mass equal to at least 20 solar masses. The astronomers concluded from its motion through space that the supergiant is about 8000 light years away and also has a companion of mass three times the solar mass or more which would fall within the limits of the masses for a black hole.

In 1973, the X-ray satellite named Copernicus registered the sharp decrease of X-rays from Cygnus XR-1 every 5.6 days which seems to be precisely the time taken by the unseen companion of Cygnus XR-1 to make one revolution around its massive partner. Every 5.6 days, the "black hole" goes behind the supergiant the flow of X-rays is briefly cut off and this is said to be the reason for the variations in X-ray intensity determined by Copernicus. While more evidence may be necessary to substantiate the hypothesis, the binary system of Cygnus and the behavior is the best evidence yet for the existence of "black hole". X-ray astronomy and the satellites like "Uhuru" and "Copernicus" are yet working hard to provide us

with more and more startling results to clear our understanding of not only X-ray sources but also of binary systems, neutron stars, and "black holes".

X-RAY ASTRONOMY
REFERENCES*

1. R. Giacconi in Varenna Summer School, XXXV, High Energy Astrophysics, Ed. L. Gratton, Academic Press, Inc. New York (1966), p. 73.

2. T.C. Weekes, High-Energy Astrophysics, Chapman and Hall Ltd. London (1969), Chapter 8.

3. R. Giacconi et al., Annual Reviews of Astronomy and Astrophysics 6, 373-416 (1968).

4. X-ray Astronomy, Ed. R. Giacconi and H. Gursky, D. Reidel Publishing Company, Boston (1974).

5. E.T. Bryam, T.A. Chubb, and H. Friedman, Science, 152, 66 (1966).

6. H. Friedman, E.T. Bryam, and T.A. Chubb, Science 156, 374 (1967).

7. Highlights of Astronomy, Ed. L. Perek, Springer-Verlag, New York (1968), pp. 178-227.

8. L. Goldberg, Annual Reviews of Astronomy and Astrophysics 5, 279-324 (1967).

9. P. Morrison, Annual Reviews of Astronomy and Astrophysics 5, 325-350 (1967).

10. H. Gursky, Developments in Applied Spectroscopy, Vol. 10 Ed. Perkins et al., Plenum Press, New York, 1972 (pp. 217-231).

11. R.J. Gould, American Journal of Physics, 35, 376-393 (1967).

12. High Energy Astrophysics, Edited by C. DeWitt, E. Schatzman, and P. Veron, Gordon and Breach, New York 1967, Volumes I and II.

13. L.E. Peterson, Annual Reviews of Astronomy and Astrophysics 13, 423-509 (1976).

*References 8 through 13 though not cited in the text are additional sources of discussion on X-ray astronomy for detailed treatments of the topic.

RADIO ASTROPHYSICS

1. Introduction

Radio Astrophysics has become one of the most productive branches of Astrophysics for providing a vast range of information on celestial bodies during the last twenty years. The study has led to a deeper understanding of astrophysical phenomena and their cosmological significance. The field divides itself into two distinct types of observations: (i) studies of radio emission from celestial bodies and (ii) analysis of radar echoes from these bodies from radio pulses transmitted from earth. The techniques of radio astronomy have yielded a wealth of information, one followed by another in rapid succession, especially since the war. Besides pure scientific interest, there are a number applications for these radio astronomical techniques.

As an example, the study of the sun which is our closest star has contributed importantly to our understanding of terrestrial magnetism, the aurorae, and radio propagation over considerable distances by ionospheric reflections. Radio spectra and radio temperatures can be measured on sources that are too far away for any optical measurements even with the largest optical telescopes. Despite its advantages, radio astronomy is faced with several problems in its use. The signals are rather weak and the techniques for receiving such weak signals have been undergoing considerable improvement

to increase sensitivity. The angular resolving power of any electromagnetic receiver, optical telescope and radio telescope alike depends upon the size of the receiving aperture in relation to the wavelength of the radiation received. Since even the shortest practical radio wavelengths are more than a factor of 10^4 greater than optical wavelengths received by conventional telescopes, a radio telescope would need to have a receiver several miles in size to equal the resolution of the largest optical telescopes. Consequently, poor resolution is a characteristic disadvantage of the average radio telescope.

We will focus our attention first on the properties of the radio waves and the design of the radio telescopes that are the analogs of the optical telescopes.

2. Radio Waves

The so called "radio channel" comprises electromagnetic waves of lengths ranging from $\sim$ 1 cm to $\sim$ 30 meters. The radio waves have added significantly to our knowledge of the cosmos as they can travel through most of the galactic matter and are not absorbed by gas and dust like the optical wavelengths. With optical waves we can see 10,000 light years in the galactic plane, but with radio waves we can see the whole galactic diameter (of $\sim$100,000 light years). This ability of radio waves to transit the entire galaxy has made radio astronomy an essential tool in studying the structure of our own Galaxy.

Radio wave emissions have been detected from the planets, the sun, and beyond the solar system. The sources beyond the solar system consist of (a) galactic arms and center, (b) supernova remnants, (c) Quasars, (d) radio galaxies external to our galaxy, and (e) ionized hydrogen clouds. For the study of these wavelengths emitted by the various sources, analogous to the optical telescopes, we need the radio telescopes which are sensitive receivers with all accessories to receive, amplify, and detect even the very weakest signals. Such developments in the design and construction of powerful radio telescopes have taken place during the last several years and major centers for radioastronomical research have been established in various countries. As a first step in our discussion of this topic, we will therefore study the general features of the radio telescopes so vital to observations in this range of wavelengths. For a historical perspective of radio astronomy and radio telescopes the reader should refer to the works of Hey[1, 2].

3. Radio Telescope

Detection and analysis of radio waves is carried out with a radio telescope. Basically such an instrument consists of (i) an antenna that collects the energy from the incident radiowaves, (ii) a transmission line through which the collected energy is delivered to a receiver, and (iii) a receiver in which the electromagnetic oscillations of the incident waves are filtered and detected after amplification by

several orders of magnitude. In view of the weak nature of the signals from celestial sources, the antenna which collects the energy from the radio waves plays a major role in a radio telescope. Let us first consider the different types of antennas that are used.

The antenna of a radio telescope is analogous to the lens or the mirror of an optical telescope. The type of antenna to be used will depend on the special requirements in terms of its uses in radio astronomical studies. The most important criteria are the high sensitivity for the very small flux densities of cosmic radio sources and adequate resolution. These two criteria can be fulfilled by having larger apertures for the antennas. Also, in order to observe sufficiently large regions of the sky, a certain degree of steerability of the antennas is needed. In general, radio telescope antennas fall into three distinct groups depending on their mechanical steerability. They are (a) completely steerable types (b) partially steerable types, and (c) fixed types.

The large radio telescopes commonly make use of huge parabolic or spherical reflectors or arrays of large numbers of elemental antenna types such as dipoles. The major antenna's are (i) 210 ft. parabolic reflector of the Australian CSIRO telescope, (ii) the ones at Jodrell Bank Radio Observatory in England, and (iii) the 300 ft diameter parabolic reflector at the National Radio Astronomy Laboratory in Green Bank, West Virginia, and the huge fixed

parabola at Arecibo, Puerto Rico. There are several other parabolic reflectors and elemental types of antenna arrangements in existence at various centers. For a fuller discussion of the theory and listing the student should refer to the text by Kraus.[3] In addition to parabolic types, spherical reflectors with necessary corrections for spherical aberration are also used in many installations. The antenna designer has to take into account a number of factors and theoretically evaluate the performance characteristics before a definite design can be chosen. However, it is not the aim of this module to discuss these details. The interested reader is referred to familiar texts on antenna theory. As was mentioned earlier, sensitivity and resolution are the main criteria.

In the radio telescope, the next most important component is the radio telescope receiver. These receivers are basically similar to the receivers in other branches of radio science and engineering. However, it must be remembered that the power level of the signal is usually quite small, of the order of 10^{-15} to 10^{-20} watt and the background "noise" level may be much higher in many cases. Therefore, high sensitivity and high stability are important requirements.

The most common type is a superheterodyne receiver. Fig. 1 gives a schematic arrangement of a superheterodyne radio-telescope receiver including the data recording system. The section after the "mixer" is the same for all frequencies whereas the RF amplifier,

the "mixer", and the local oscillator must be designed appropriately for the range of frequencies to be studied. Also, receivers may be conveniently divided into two groups viz., "continuum receivers" and "spectral line receivers". While the exact frequency of operation is not critical for the first type, for the latter type provision for precise tuning to the frequency that is to be observed is very critical. Multichannel receivers are used extensively in radio-astronomy. For a detailed review of the receivers in use, refer to the text by Kraus[3].

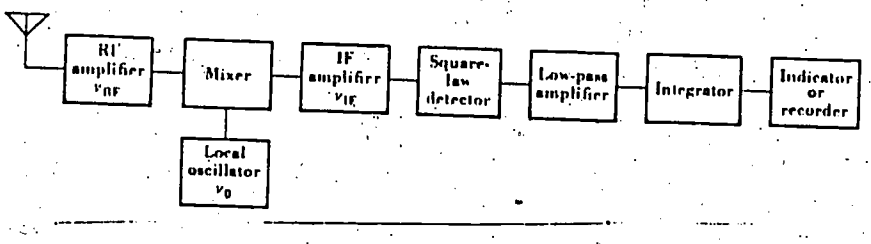

Fig. 1. A Superheterodyne Radio Telescope Receiver

Fig. 2. shows the block diagram of a simple interferometric receiver where two or more antennas are separated from each other by distances of several wavelengths. The two antennas receive the same signal because the antennas are pointed in the same direction. However, the two signals will have a phase difference depending on

the direction of the source of radio waves. The two antennas have their own associated separate amplifiers. Sensitivity of these receivers may be improved by signal correlation techniques which are special data processing methods.

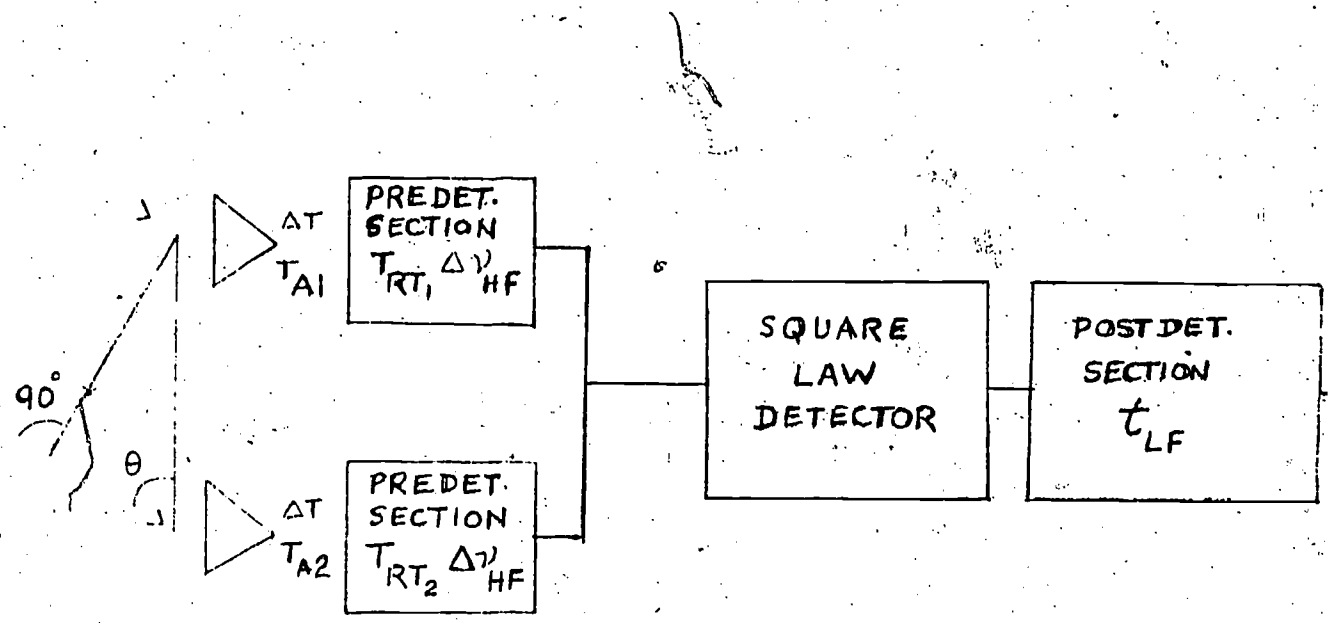

Fig. 2. Simple Interferometer Receiver

Another essential component in a radio telescope is the amplifier. These are low-noise amplifiers which are commonly used as RF pre-amplifiers to obtain the requisite sensitivity. Parametric amplifiers, masers, and tunnel-diode amplifiers are special low-noise types of amplifiers used in radio astronomy. The masers and parametric amplifiers are relatively narrow band-width devices, while for broad-band devices tunnel-diode amplifiers are chosen. Parametric amplifiers use a nonlinear reactance element to achieve amplification.

Such a nonlinear element may be a varactor (or a variable capacitance diode) like a p-n junction diode with voltage-dependent capacitance. The parametric amplifiers are practically devoid of internal noise and constitute a new useful category of amplifying devices. The new very high frequency amplifier using induced emission of atoms to produce amplification called the maser amplifier has come into greater use in radio telescopes. (The maser is actually the forerunner of the more familiar laser and operates in the radiofrequency spectrum whereas the laser operates at optical wavelengths.) In a maser amplifier (e.g. ruby crystal with chromium impurity), the quantum energy states of an atom are used for amplification. These have definite advantages in terms of the gain mechanism and the low operating temperatures. Fig. 3. shows the records of signal from Cygnus A with an ordinary receiver and also with the addition of a maser, the latter resulting in an appreciable reduction in receiver-noise fluctuations.

The above discussion on the general features of the radio telescopes would be incomplete without the mention of the antennas used for measuring the state of polarization of the waves of cosmic origin. There are four parameters that are to be measured in connection with polarization and they are (i) intensity of the unpolarized component, (ii) the intensity of one linear or right-handed circular component, (iii) the intensity of the other linear component perpendicular to the

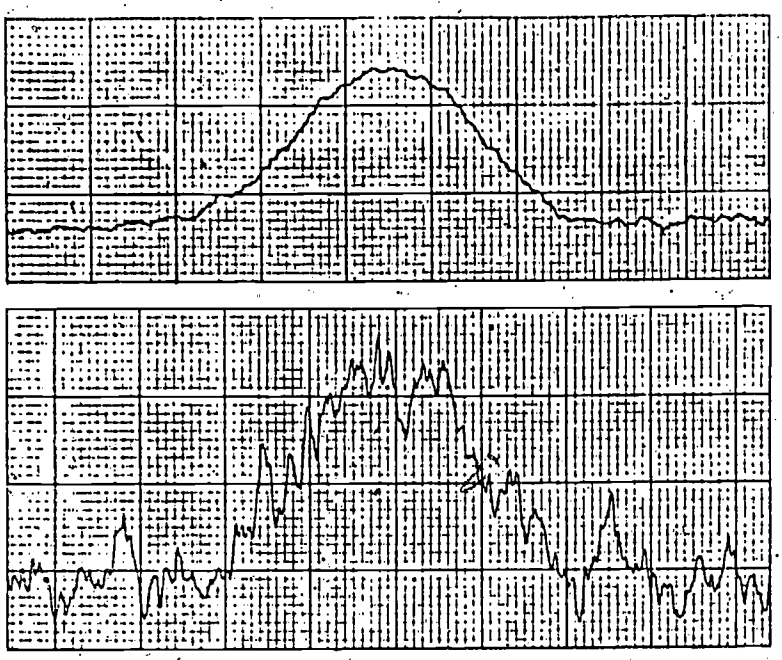

Fig. 3. Records of Cygnus A (a) Ordinary Receiver (b) Same With a Maser

first or the left-handed circular component, and (iv) the relative phases of the two components. In the case of the radiation from the sun the problem is easy because of the strongly polarized radiation. But the problem is difficult in the case of weakly polarized and faint signals from the galactic and extragalactic sources. For such purpose, a linear polarized antenna may be rotated about the pointing direction and the variation in the energy received may be studied. Sometimes, two differently polarized antennas may also be used and the correlation of the two polarized components may be measured. Since there are several instrumental factors to control the precise

measurements of the states of polarization of the radiation from radio sources are still in need of improvements to obtain astrophysically significant results. For descriptions of radio telescopes one can also use as a guide the book by Christiansen and Hogbom,[4] and other sources.[5,6]

4. Mechanisms for Emission of Radio Waves

There are three principal mechanisms for continuum emission of radio waves. They are: (i) thermal emission from sources radiating like classical blackbody radiators, (ii) thermal emission from ionized gases, and (iii) emission from electrons with relativistic energies under the influence of a magnetic field (magnetic bremsstrahlung or Synchrotron radiation). Other types of radio waves emission mechanisms have also been postulated. However, the above three account for most of the observed radio waves and therefore let us discuss them briefly.

(i) Thermal emission from blackbody radiators is characterized by the Planck's law of radiation which gives the brightness $B(\nu)$ of a blackbody radiating a frequency ν at temperature T°K as

$$B(\nu) = \frac{2h\nu^3}{c^2} \cdot \frac{1}{e^{h\nu/kT} - 1} \qquad (1)$$

In the radio wavelength region, $h\nu \ll kT$ since we are dealing with very large wavelengths and very low frequencies, the above relation reduces to

$$B(\nu) = \frac{2h\nu^3}{c^2} \cdot \frac{kT}{h\nu} \propto T\nu^2 \propto T\lambda^{-2} \qquad (2)$$

It must be noted the radiation from the blackbody radiators is rather weak. The thermal radiations from the moon, Mars, and other planets have been detected and the brightness has been found to be inversely proportional to the square of the wavelength consistent with Eq. (2). The continuous spectrum is unpolarized.

(ii) Thermal emission from ionized gases is caused by the detached electrons in an ionized gas. While the line emissions are associated with transitions between the discrete bound states of atoms or molecules. the continuum originates from the acceleration experienced by the free electrons when deflected in passing near a proton. Such fluences on the free electrons are temporary and the interaction or approach results in a "free-free" transition in contrast to the "bound-bound" transitions in atoms or molecules. As an example, for diffuse hydrogen, the absorption coefficient is given by

$$K \propto N^2 T^{-3/2} \nu^{-2} \qquad (3)$$

N being the free electron density. The flux density is proportional to $\lambda^{-2}\nu^{-2}$ and the spectrum for the Orion nebula is consistent with that type of dependence.

(iii) Synchrotron emission is believed to be the mechanism for

continuum emission in the radio wave length region for most of the nonthermal radio sources. In a radio source, the magnetic fields are very weak and the relativistic electrons interacting with the magnetic fields give rise to radio waves. In a simplified treatment of the problem, the radius R of the path of a particle of charge e and mass m moving perpendicular to a magnetic field B is

$$R = mv/Be \quad \text{and} \quad \nu = \frac{v}{2\pi R} = \frac{Be}{2\pi mv} \tag{4}$$

For interstellar magnetic fields B is 10^{-9} to 10^{-10} w/m^2 and therefore ν is in the range 140 to 14 cps. When the electrons have relativistic energies the radiation from the particle is concentrated in a cone of angle

$$\theta = 2\sqrt{1-(v/c)^2} \tag{5}$$

For 10^9 eV energy, θ is 10^{-3} radian or 3.4 min of arc. The observer in the plane of the orbit will receive from the electron pulses of length

$$\Delta t \simeq \frac{R\theta}{c}\left[1-(v/c)^2\right] \tag{6}$$

The radius of the path is

$$R \simeq c/2\pi\nu \tag{7}$$

and thus

$$\nu = \frac{Be}{2\pi m_0}\sqrt{1-(v/c)^2} \tag{8}$$

m_0 being the rest mass of the electron. One can see that when $v \to c$, $\nu \to 0$ as $R \to \infty$. The value of pulse time

$$\Delta t \simeq \frac{2m_0}{Be}\left[1-\left(\frac{v}{c}\right)^2\right], \tag{9}$$

and

$$\nu_{max} \simeq \frac{1}{2\pi\Delta t} = \frac{Be}{4\pi m_0} \cdot \frac{1}{\left[1-(v/c)^2\right]} \tag{10}$$

As an example, for electrons with energy of 1 GeV, and $B = 10^{-5}$ Gauss, ν_{max} is 60 Mc. The synchrotron radiation is linearly polarized with the direction of the electric vector parallel to the orbital plane of the electron.

While we have considered in the above discussion only three mechanisms briefly, it must be noted that there are other various mechanisms of radio emission like the oscillations of ionized gas, gyromagnetic emission, hyperfine structure of interstellar hydrogen, and Cerenkov radiation accounting for line emissions. As can be seen from the Table below[3], the various mechanisms present diverse characteristics. For a fuller treatment of all mechanisms one should discuss the laws of emission and absorption, radiation transfer in a gas, and fundamentals of Cerenkov radiation. However, for our present scope we shall review very briefly the most interesting results obtained from several radio sources.

Table 1. Summary of Various Mechanisms of Radio Emission

Type of Radiation	Origin	Excitation temperature	Spectrum	Polarization
21 cm line	Interstellar neutral hydrogen	(100 to 130°K)	Narrow line shifted or widened by Doppler effect	Unpolarized
Black body emission	Moon, planets	Equals absolute temperature	Continuous spectrum	Unpolarized
Thermal emission from ionized gases	Interstellar ionized hydrogen	(10^4°K)	Continuous spectrum with absorption coefficient varying as ν^{-2} and N_e^2	Unpolarized
	Solar corona	(10^6 to 10^7 °K)		
Plasma oscillations	Sun	(10^{10} to 10^{11} °K)	Fundamental (frequency varying as $N_e^{1/2}$) + harmonics	Usually unpolarized
Gyromagnetic emission	Sun	very high	Fundamental (frequency varying as B) + harmonics	Circularly polarized
Synchrotron emission	Sun	$>10^{11}$ °K	Very wide spectral band	Linear or circular polarization
	Radio sources	Always very high	Continuous Spectrum	Linear in some cases
	Interstellar space	Very high	Continuous spectrum; brightness temperature varying as $\nu^{-2.7}$	Linear in some cases
Cerenkov radiation	Sun?	Very high	Narrow band	

5. 21 cm Line of Hydrogen

The greatest advance in radio astrophysics has been as a result of the observation of the emission of 21 cm wavelength line. The vast amount of data that this single discovery has contributed over the years to the understanding of our own galaxy as well as many other astrophysical phenomena is very significant and deserves detailed discussion as a separate topic by itself. However, we shall review only briefly the origin of this important emission and its contributions to astrophysics.

The possibility of observing such a transition of neutral hydrogen in interstellar space was theoretically predicted by van de Hulst as early as 1945 and experimentally was first detected by Purcell in 1951[7]. The line has its origin in the transition between two hyperfine levels of the ground state of neutral hydrogen in which the magnetic moments of the proton and electron are antiparallel and parallel. The transition with a frequency of 1420.4 MHz is a magnetic dipole transition ordinarily classified as "forbidden transition" and the radiative lifetime of the upper level is very long ($= 1.1 \times 10^7$ years). The line derives its particular significance from the fact that it is the only means of directly observing netural hydrogen in the groundstate since optical observations cannot be used to estimate the population of the ground level where practically all of the hydrogen atoms are in the interstellar matter. Further, unlike the optical methods which

are affected by the interstellar dust clouds causing obscuration, the radio observations are not affected and can be used with advantage to study even the remote parts of the galaxy.

First of all the most important contribution of the 21 cm line studies to the knowledge on the galactic structure is the detailed mapping of the distribution of neutral hydrogen in the plane of the galaxy by obtaining the line profile. The bulk of the hydrogen was found to be contained in a flat thin disk. The outlines of large hydrogen clouds in which the stars are formed have been mapped through the observations of 21 cm line. That the Milky Way is a great spiral of stars whose arms swirl out from the center was also inferred from such observations. The spiral arm structure together with the determination of the galactic rotation gave the complete picture of the galaxy including the distances, densities, and velocities of the neutral hydrogen clouds. Fig. 4 shows the spiral arms of the galaxy.

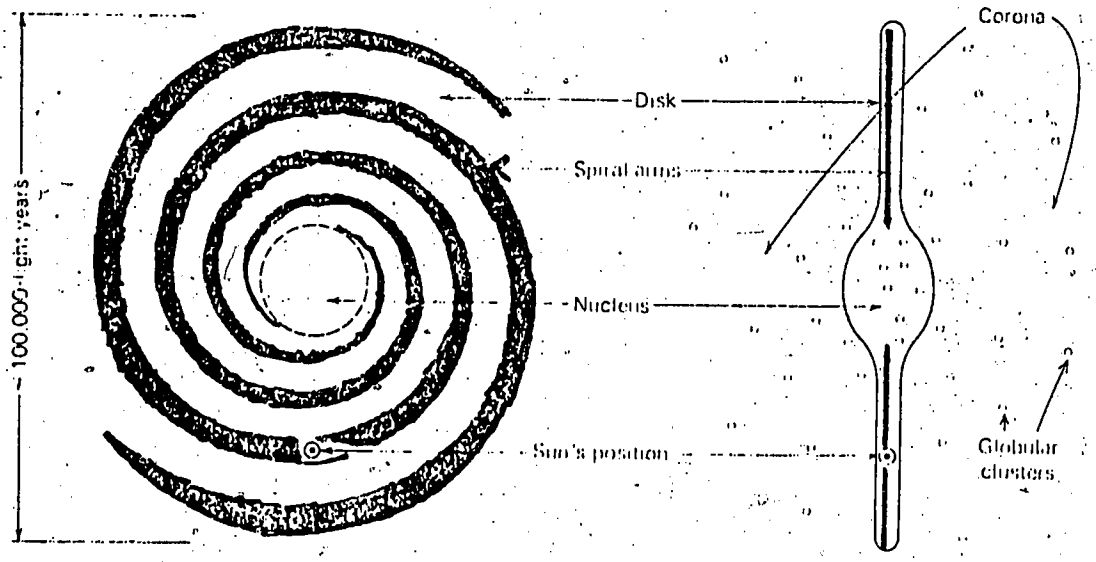

Fig. 4. Spiral Arms of the Galaxy

6. Radio Emissions From the Solar System

The studies of the solar atmosphere and sun spot activity have always attracted the attention of astrophysicists in general and radio astronomers in particular. After the initial observational and theoretical work on thermal radio emission from the solar atmosphere, the first significant step was the determination of the radio contour map of the quiet sun (period of minimum sunspot activity). As expected

the optical and radio spectral data complementing each other gave values of electron density and temperature and thus about the conditions of the solar chromosphere and corona in good agreement. The radio emission following certain large solar "flares" and labelled microwave outbursts has been identified with synchrotron radiation from trapped electrons that accelerated to relativistic speeds in the magnetic fields of the active region.

Radio emission has been observed also from other planets, notably the strong signal from Jupiter. The temperatures of the planets like Jupiter, Venus, and Mars have been estimated from the radio waves emerging from these planets and their intensities. Radio waves from Saturn, Uranus, and Neptune also have been detected. The temperatures recorded at some wavelengths have been higher than expected. Another interesting result has been the "greenhouse effect" attributed to the atmosphere of Venus in an attempt to explain the differences in temperatures of 400°K and 600°K obtained using 8 mm and 10 cm waves. Since presumably the 8 mm waves originate from cooler points of the atmosphere and the 10 cm radiation was shown to come from the solid surface, the vast amounts of carbon dioxide in the Venus atmosphere would account for the "greenhouse effect".

7. Supernova Remnants

One of the most powerful radio emitters beyond the sun is the

constellation Taurus A that coincides with the Crab nebula. The study of the Crab nebula actually marked the beginning of bridging optical and radio astronomy. It was suggested that in the Crab nebula both the optical emission and the radio emission may arise from the same mechanism viz. synchrotron emission. The validity of this hypothesis was established from polarization measurements of optical radiation and the 3 cm wavelength. More importantly, the discovery pointed to the type of astrophysical phenomenon associated with intense radio sources viz. the unusual explosive activity. This led to the search for radio emissions from other supernova remnants. The remnants of Tycho Brahe's supernova of 1572 was studied and radio mapping at $\lambda = 21.3$ cm was completed in 1967. Another remnant as a powerful radio waves emitter is Cassiopeia A (Cas A). It is believed that in the evolution of the various stages of the supernovae, these remnants are powered by neutron stars that produce relativistic electrons and these electrons interact in the nebula to produce radio emissions, visible light, and X-rays. Thus the radio astronomical studies of these remnants provide an insight into the evolution of these things including the pulsars to be discussed next.

The schematic of the evolution of a supernova remnant responsible for emission of radio waves and X-rays is shown in Fig. 5. At the outset, the star is in a pre-supernova stage. This is followed by the

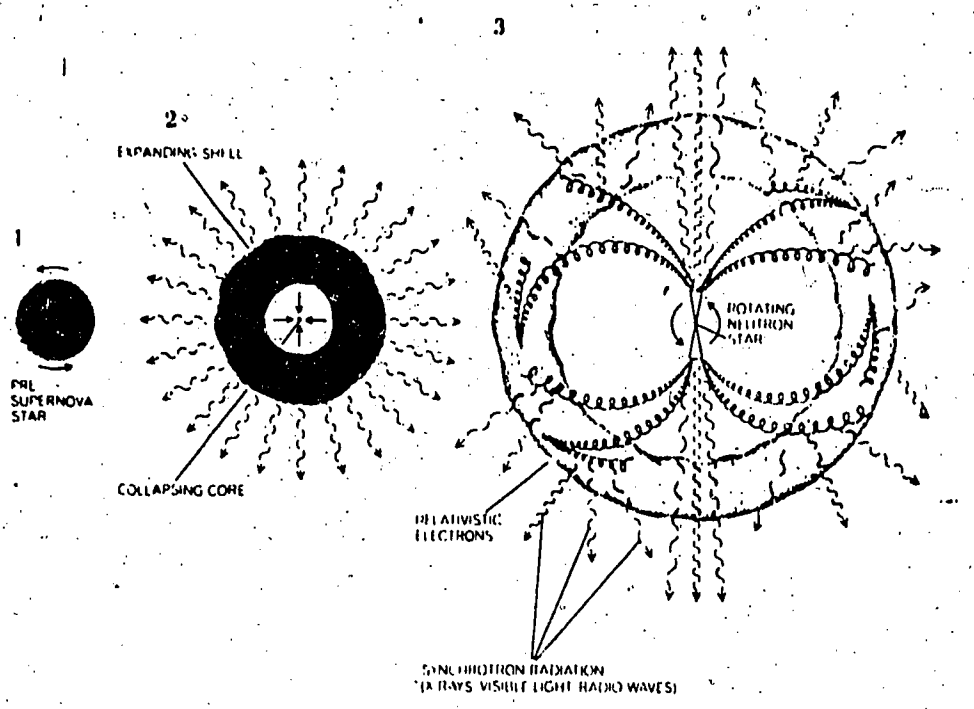

Fig. 5. Supernova Explosion and Radio Emission

sudden collapse of the core to form a highly magnetized rapidly rotating neutron star with simultaneous ejection of matter with tremendous velocities into the interstellar medium. The rapidly rotating neutron star produces in the next stage the electrons at relativistic speeds. By synchrotron process these relativistic

electrons give rise to radio waves. During the first thousand years or so following the explosion, the radio emissions as well as optical and X-ray emissions are observed together with pulsed radiation due to the rotational speed of the neutron star. The Crab nebula and the associated pulsar (labelled NPO532) are at this stage. With the loss of the rotational kinetic energy, the rate of slow down of the pulsar gives approximately 1000 years as the age which is in good agreement with the known age of the Crab nebula. Also, from the expansion of the shell with the formation of shock wave, the relativistic electrons left over from the active phase will produce radio waves on interaction with the high magnetic field behind the shock.

8. Pulsars

The discovery of the pulsating radio sources which seem like beacons broadcasting time signals is another most astonishing event in the progress of radio astrophysics. These are detected using large aerials at meter wavelengths. Nearly 150 pulsars have been discovered following the first one CP1919 recorded by the Cambridge team.[8] The rapidity of the pulses gave the preliminary clue to the nature of these emitters suggesting they should be from an extremely small condensed object. Gold[9] proposed the hypothesis that a pulsar is a neutron star that is rotating at a fast rate with a very high magnetic field ($\sim 10^{12}$ Gauss) resulting from the contraction of the original field of a collapsing star. Also, it was predicted that with lapse of time

the pulse repetition rates would slow down. The study of the supernova remnants confirmed such hypothesis and predictions. For example, the extended radio source Vela X believed to be the debris of a supernova explosion has a period of 89 milliseconds compared to 33 ms of the pulsar NPO532 in the Crab nebula. The latter being the fastest is the youngest pulsar known thus far. As mentioned ea- .ier, the rate of slowing down of the pulsar puts the age of the Crab nebula at nearly 1000 years. The Crab nebula and the associated pulsar have been studied in great detail from observations using rockets, balloons, satellites, and ground-based stations. The identification of the above pulsar as also the first X-ray pulsar has stimulated further activity in the realm of the experiments.

9. Radio Spectral Lines Due to Molecules

The observations of the 18 cm hydroxyl (OH) lines in 1963 marked the first significant step in the detection of molecular lines by radio astronomical methods. The 18 cm line results from the dipole-allowed transitions between the hyperfine structure of the two levels (resulting from Λ doubling) of the lowest electronic, vibrational, and rotational energy of the molecule.[10, 11] These transitions are shown schematically in Fig. 6. Since they are dipole transitions, they are 10^4 stronger than the 21 cm line which is a "forbidden transition".

Interstellar OH lines were observed from radio source Cassiopeia A and Sagittarius A. The strong intensities, polarization, and narrow

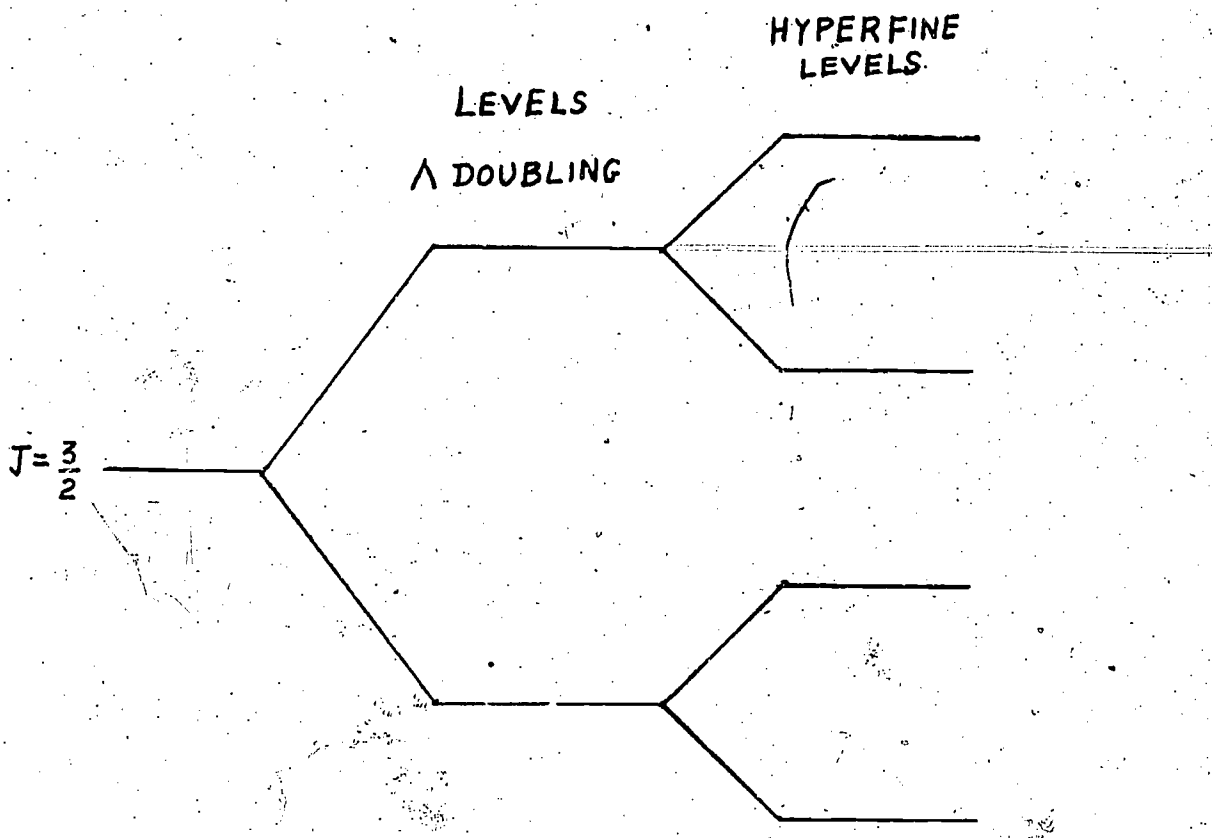

Fig. 6. $2\pi_{3/2}$ State of OH Molecule

bandwidths of OH emission suggest the possibility of some kind of maser action involving pumping at one frequency and stimulated emission of radiation at radio frequencies. The OH lines provide also a useful tool for estimating the abundance of oxygen vs hydrogen.

Following the observation of OH lines other molecular lines in the radio frequency region have been observed. NH_3 was detected by the Berkeley team in 1968. Soon other interstellar molecules have been identified using radio astronomical techniques and detailed

comparisons have been made with rotational spectral and microwave spectral data.[12] As examples the molecules HCN methyl alcohol (CH_3OH), formaldehyde (CH_2O) and dimethyl ether (CH_3OCH_3) should be mentioned. The list of molecules in the galactic environment[13] is still growing rapidly and the study of molecular abundances in space has received a new and great impetus from the techniques of radio astrophysics. It is also interesting that polyatomic molecules, many of them of considerable biochemical interest, do survive in the interstellar environment contrary to expectations. These identifications have provided more questions, clues, and scope for elucidating the formation of stars. The study of the synthesis of molecules in space is of great cosmological significance to our understanding of the nature, origin, and future of the universe.

10. Radio Galaxies

Many normal galaxies and their radio characteristics have been studied since 1959 and their neutral hydrogen content estimated using the 21 cm line. In addition, over the last nearly 20 years, the study of the external galaxies using radio techniques has been one of the principal aims of the astrophysicists in view of the special significance it has in connection with the evolution of galaxies and cosmology.[14] Since optical data on red shifts are the only means of estimating great distances, necessarily in all cases the comparison of radio astronomical data with optical information has been very essential to

understanding the astrophysical processes involved.

The most powerful of radio galaxies identified so far is Cygnus A at a distance of about 550 million light years. The structure of this source has been studied and the detailed contour map[1] has shown the existence of double structure. Another radio galaxy which has also been studied in detail is Centaurus A. Several things have emerged from such observations. In the first place, the mechanism of radio emission has been established to be the synchrotron radiation accounting for the intensities, spectra, and the polarization characteristics. The magnetic field directions have been deduced from the radio studies. These radio galaxies with their multiple structures (e.g., Cygnus A) do not fit into the Hubble's group of normal galaxies. The extended features (beyond the optical galaxy) indicate that the high energy particles and fields responsible for radio characteristics are thrown outward and are considered to be the result of an expansion from a past explosion in the optical galaxy. The vast release of energy and the optical evidence of violent events in the galactic nuclei are fundamental questions concerning the nature of these sources.

II. Quasars

The quasistellar radio sources or quasars as they are called, were first discovered in 1963 and perhaps form the most important as well as intriguing problem in extragalactic astronomical research. The radio spectral data and the optical emission lines with appreciable

red shifts have shown that these are very compact sources. For example, the spectra of 3C273 was noticed to consist of highly red shifted absorption and emission lines (e.g. H_{α} line appearing in the infrared region) and remained a puzzle in the quasar story until the mystery was solved later. The lines of 3C48 corresponded to an even larger shift of 0.367.

From their optical magnitudes and distances of billions of light years, their optical luminosities must be very large. They are as bright as 100 normal galaxies. The distance of 3C273 is derived to be 1.6 billion light years from the Hubble's law of red shifts and similarly 3C48 is inferred to be 3.6 billion light years away. The quasar OQ172 is estimated to be speeding at 90% of the velocity of light and at the limits of the observable universe. The discoveries of several quasars had followed and the study of the properties of these radio sources at high galactic altitudes supplemented by optical and X-ray data will lead to an integral picture.

12. Conclusion

There are many other features that have been contributed by radio astronomy to greatly advance our knowledge of the universe covering such diverse areas as cosmology, evolution of galaxies, galactic magnetic fields, high energy particles and the like. The progress in experimental techniques and sophisticated instrumentation certainly forces the focus of the optical astrophysicist to new and

exciting phenomena. The radio methods have achieved extremely high angular resolution comparable to and even better than any optical telescope. The study of most of the very distant sources has to depend entirely on the radio astronomical techniques. With the present trend to use the space vehicles more and more in astrophysical studies, the astonishing and rapid growth of radio astronomy in the last few years will easily place this branch of astrophysics at the forefront to unravel many other mysteries of the universe within the very near future.

RADIO ASTROPHYSICS

REFERENCES

1. J.S. Hey, The Evolution of Radio Astronomy, Science History Publications, New York (1973).

2. J.S. Hey, The Radio Universe, Pergamon Press, New York (1971).

3. J.D. Kraus, Radio Astronomy, McGraw-Hill Book Company, Inc., New York (1966).

4. W.N. Christiansen and J.A. Hogbom, Radio Telescopes, Cambridge University Press, London (1969).

5. Invisible Universe; the Story of Radio Astronomy Ed. G.L. Verschuur et al., Springer-Verlag, New York (1974).

6. J.L. Steinberg and J. Legueux, Radio Astronomy, McGraw-Hill Book Company, Inc., New York (1963).

7. A.G. Pacholczyk, Radio Astrophysics, W.H. Freeman and Company, San Francisco (1970), pp 195-205.

8. A.S. Hewish, et al., Nature 217, 709 (1968).

9. T. Gold, Nature 218, 731 (1968).

10. G. Herzberg, Spectra of Diatomic Molecules, Van Nostrand Company, Inc., Princeton (1950).

11. R.F. Barrow, Molecular Spectroscopy McGraw-Hill Book Company, Inc., New York (1962).

12. W. Gordy, R. Sheridan, and Tramburulo, Microwave Spectroscopy Dover Publications, New York (1966).

13. M.A. Gordon and L.E. Snyder, Molecules in the Galactic Environment John Wiley and Sons, Inc, New York (1973).

14. D.W. Sciama, Modern Cosmology, Cambridge University Press, London (1971).

MOLECULAR ASTROPHYSICS

1. Introduction

The study of the molecular spectra of stellar sources has contributed significantly to our knowledge in astrophysics. Molecular bands are observed in the spectra of all stars except for O, B, A type stars in which surface temperatures are so high as to prevent molecules from forming. Thus the study of molecules in stars will cover more than half of stellar astronomy. The most notable stellar molecular spectra have been of G and K stars (showing CH, CN, bands), of M stars (with TiO bands), and of carbon stars with their very strong C_2, CH, and CN bands. The vast amount of data on electronic, vibrational, and rotational energy levels of molecules has enabled a detailed quantitative analysis of many stellar sources during the last decade.

As is well known, stars with temperatures below $\sim$ 4000°K (cool stars) are characterized by extensive molecular spectra. Any attempt to study the nature of these stars would therefore involve a detailed investigation of their spectra. There are in general three main areas pertaining to such a study. The interpretation of these molecular spectra and the formulations of model atmospheres depend crucially on a knowledge of the precise energy levels and the quantum-mechanical transition probabilities. Further, the calculations of chemical compositions from the laws governing chemical equilibria are very

important especially for cool stars. The problem of isotope ratios can also be solved through study of the isotope shifts in the molecular spectra of these sources so that one can provide the information that is vitally needed about stellar evolution, as in the case of the cool red giants.

The cold dust regions include both nebular clouds and circumstellar shells. The radio observations of these regions detect the emission and absorption lines corresponding to the rotational lines of molecules. The study of these spectral lines is essential to deduce the excitation temperatures and abundances in these regions which are obscured by dust and therefore inaccessible to the usual optical methods of observation. Abundance determinations in nebular regions are particularly important because these regions are thought to be areas of star formation. Abundances in circumstellar shells of late giants and supergiants are important because they are thought to contain material returned to the interstellar medium after being processed inside a star. Further, some of the emission from OH and H_2O in these regions are found to be amplified by maser action. The detailed nature of these huge interstellar masers is still not well understood and is a subject of much current astrophysical interest.

Molecular spectral studies are also of great interest for obtaining knowledge about comets, the solar chromosphere, and other terrestrial phenomena like the night sky, aurora, twilight, etc. A large number of astrophysically

significant diatomic molecules has been studied in great detail during the last few years, and there has been a strong renewed interest in molecular spectra stimulated by recent astronomical applications. It is the purpose of this course to consider the basic principles of diatomic molecular spectra and then to discuss some important applications in astrophysics, as examples of the usefulne - molecular spectroscopy.

2. Energies of Molecular Systems

Although both diatomic and polytomic molecules have been identified in various stellar sources, study of the spectra of diatomic molecules is a good introduction to a subject that is of immense value for the interpretation of the various physical processes giving rise to the spectra of stars and other stellar bodies. Hence, for this module we will consider as our main interest the characteristics of the spectra of diatomic molecules. Since the observed spectra represent energies emitted or absorbed in transitions of the molecular system between levels each of which is characterized by a particular value for the molecular energy, it is necessary to review briefly the theoretical considerations for evaluating molecular energies in different electronic and excited states.

The total energy of a diatomic molecular system consists of (i) the electronic energy resulting from the nucleon po-

tential energy and the electronic potential and kinetic energies, (ii) the vibrational energy due to the oscillations of the nuclei of the system, and (iii) the energy due to the rotation of the molecule about an axis. Therefore, one has for the total energy of the molecule

$$E_{total} = E_{electronic} + E_{vibrational} + E_{rotational} \quad (1)$$

Figure 1 shows the energy levels of a diatomic molecular system schematically for two different electronic states E_1 and E_2 characterized by the corresponding two potential energy curves. The curves give the potential energy as a function of the distance r between the two nuclei of the diatomic molecule in each electronic state.

It may be seen from Figure 1 that each electronic state has associated with it an electronic energy E_{el} (corresponding to the energy for the minimum of the potential energy curve) with respect to the minimum of the ground state (E_1), a vibrational energy E_{vib} depending on the vibrational quantum level v (with single prime for denoting the upper electronic state and double prime for the lower electronic), and a rotational energy E_r depending on the moment of inertia of the molecular system in the specified quantum level.

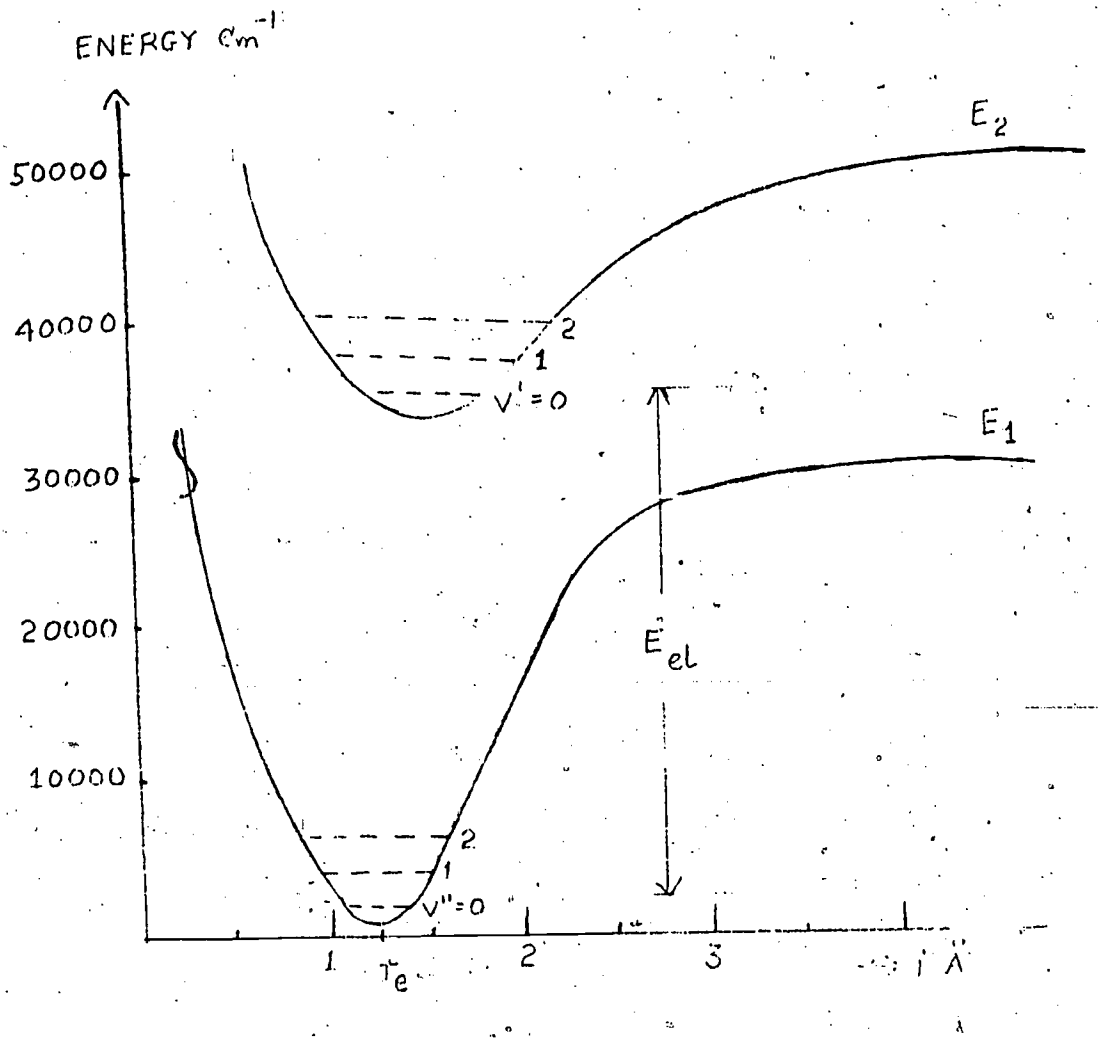

Figure 1. Potential Curves for Electronic States

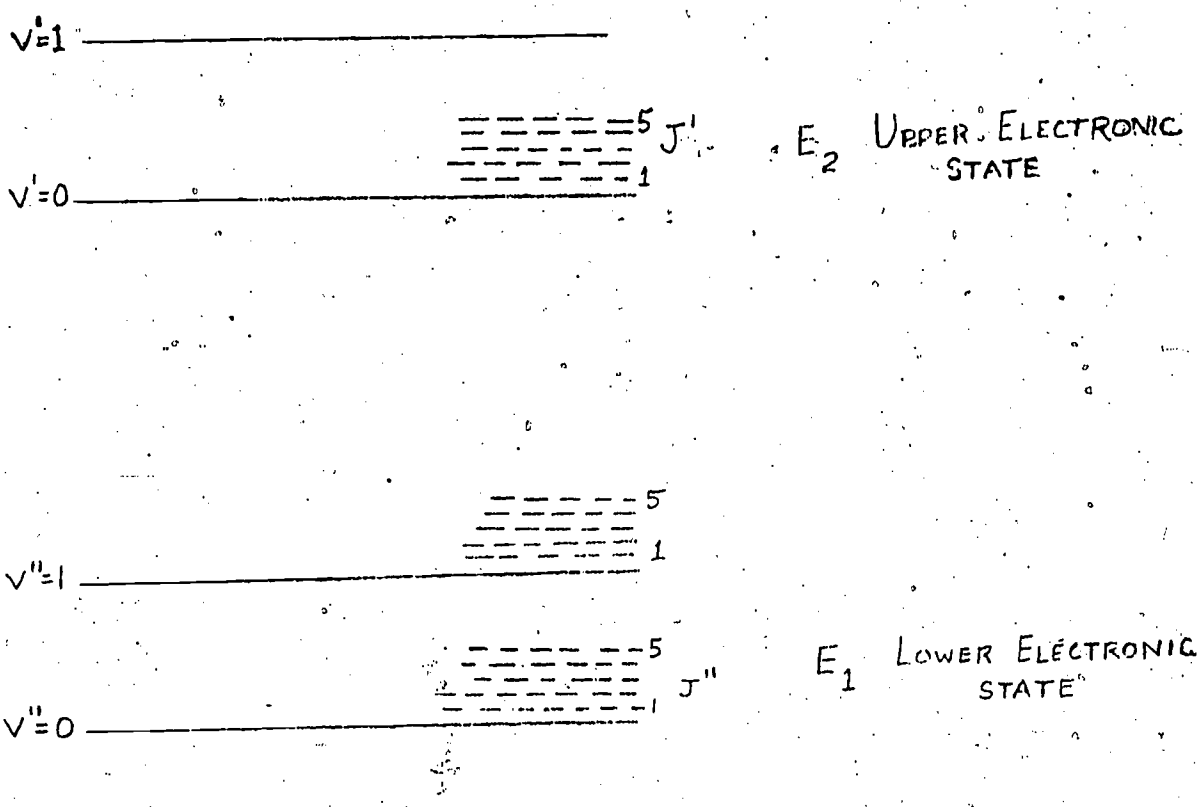

Figure 2. Vibrational and Rotational Levels

For example, the energy for the level in the upper electronic state with v' = 1, J' = 1 will be

$$E_2 = E_{el} + E_{vib}(v' = 1) + E_{rot}(J' = 1). \quad (2)$$

E_{el} is the energy difference between the minima of the two potential energy curves. As will be shown later, the energies for the vibrational level v' and the rotational level J' will depend on the vibrational frequency ω of the molecule and the moment of inertia I of the molecule, respectively, as well as on the respective quantum numbers. The electronic energy for the ground state (E_1) is zero and one considers the vibrational energy (due to v", ω") and rotational energy (due to J" and I") only. Thus, for the molecular transition from state 2 to state 1, the energy difference will be

$$E_2 - E_1 = [E_{el} + E_{v'} + E_{j'}] - [0 + E_{v"} + E_{j"}] \quad (3)$$

The frequency observed in the spectrum of the molecule will be

$$\nu = (E_2 - E_1)/h \quad (4)$$

where h is the Planck's constant. The spectral region in which the transition is observed will depend on the energy difference $E_2 - E_1$. If the transition is between two

electronic states is mentioned above, the energy differences will be large and hence, the transition may be observable in the visible or ultraviolet. But if the transition is between levels of the same electronic state, the energy difference will be small and the transition will be observable in the infrared or microwave regions of the spectrum. The typical values of the energies involved are such that $E_{el} >> E_{vib} >> E_{rot}$. For example, electronic energies are of the order of a few electron volts while vibrational energies are in the range. .01 to .1 eV and rotational energies are from .001 to .01 eV. For a molecule the total energy is written as a sum of three contributions,

$$E = E_{el} + E_{vib} + E_{rot} \qquad (5)$$

It is more conventional to write this as a sum of terms which are the corresponding energies in units of wave number (cm^{-1}) which is the reciprocal of wave lenghth in the form

$$T = T_e + G + F \qquad (6)$$

where T_e is the electronic part, G is the vibrational part, and F is for the rotational part of the molecular energy.

If the diatomic molecular system is considered to be a harmonic oscillator, the vibrations of the two nuclei may be represented by a one dimensional wave equation in terms of the force constant k and x is the displacement from the

equilibrium distance r_e. The vibrational energy levels can then be written in the simple form

$$E_v = h\sqrt{k/\mu}\ (v + 1/2) = h\nu_{osc}\ (v + 1/2)\ v = 0,1,2, \quad (7)$$

where μ is the reduced mass of the two nuclei and is given by $\frac{m_1 m_2}{m_1+m_2}$

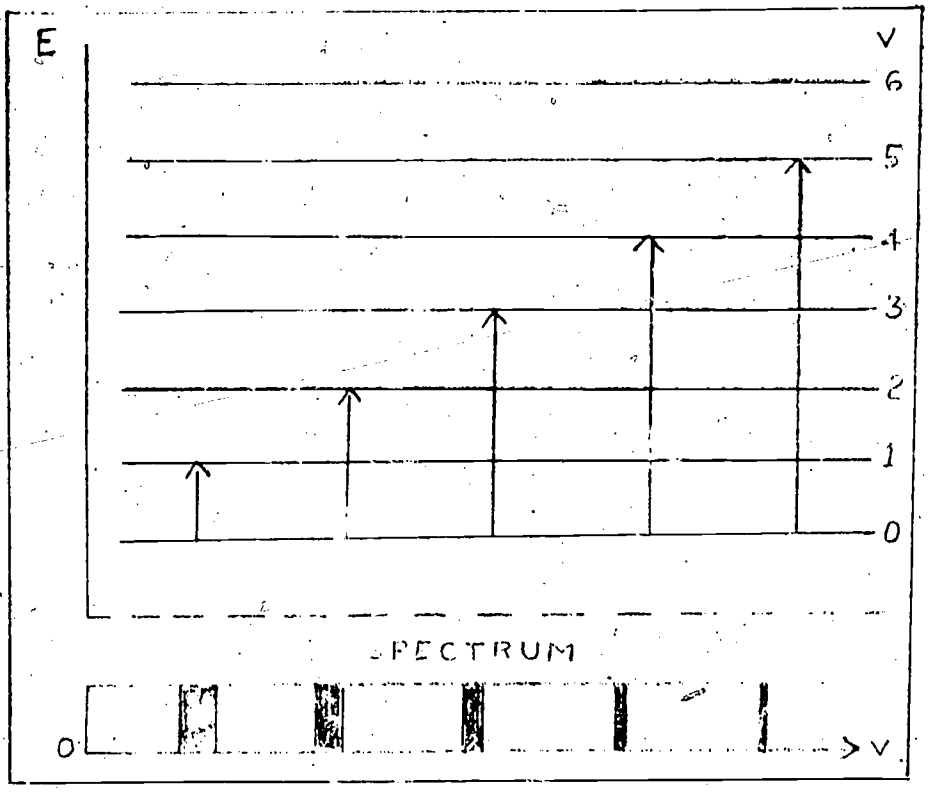

Figure 3. Infrared Transitions for Anharmonic Oscillator

v is the vibrational quantum number and the vibration frequency $\nu_{osc} = \sqrt{k/\mu}$. The vibrational term value is then written in terms of $\omega_o = \nu_{osc}/c$ as

$$G(v) = \omega_o (v + 1/2) \text{ cm}^{-1} \qquad (8)$$

The selection rule for a dipole transition between levels v' and v" is that $\Delta v = \pm 1$ and the permanent dipole moment is different from zero. For homonuclear molecules, those with identical nuclei such as H_2, there is no dipole moment, hence there are no allowed transitions and hence no infrared spectrum in emission or absorption. In deriving the selection rule, it must be noted that $\Delta v = \pm 1$ holds strictly only if the dipole moment can be expressed as $M = M_o + M_1 x$. If it is necessary to include terms involving higher powers in x, then transitions with $\Delta v = \pm 2, \pm 3, \ldots$ are also allowed.

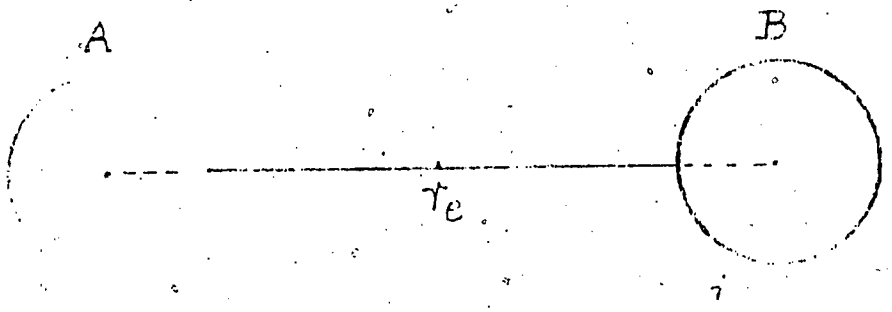

Figure 4. Diatomic Molecule

The rotational energies for a rigid rotor model of a diatomic molecule are given by

$$E_{rot} = (h^2/2I)\, J(J+1) = (h^2/2\mu r^2)\, J(J+1), \quad J=0,1,2,\ldots \qquad (9)$$

where I is the classical moment of inertia of masses m and m_2 rotating about a common center of mass, namely $I = \mu r^2$ where r is the separation of the two masses and μ is the reduced mass as before. J is the rotational quantum number and has integer values. The rotational energies in wave number units (term values) corresponding to E_{rot} will be

$$F(J) = E_{rot}/hc = (h/8\pi^2 Ic)J(J+1) = BJ(J+1) \qquad (10)$$

where B is the rotational constant $h/8\,^2cI$. The selection rule

$$\Delta J = \pm 1. \qquad (11)$$

can be derived from the properties of the solutions of Eq. (11). The frequencies observed in the spectrum of a simple rigid rotator are given by

$$\nu = F(J"+1) - F(J") = 2B(J"+1) \qquad (12)$$

with J" = 0,1,2,.... and thus the spectrum consists of a series of equally spaced spectral lines.

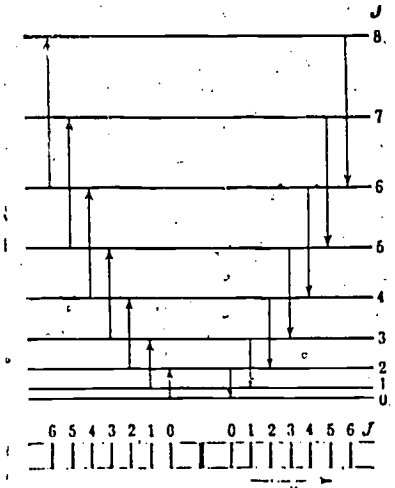

Figure 5. Vibration-Rotation Spectrum

The above discussion holds for the selection rules for the infrared spectrum of a harmonic oscillator and rigid rotor. The Raman spectrum arises from the dipole moment induced in a molecule by the presence of an electric field including that of the light wave itself. It is the only type of infrared spectrum present in a homonuclear molecule which has no permanent electric dipole moment as pointed out earlier. For the vibrational Raman spectrum, the selection rule is the same as for the infrared spectrum, i.e., $\Delta v = \pm 1$ while for the rotational Raman spectrum, the selection rule is

$$\Delta J = 0, \pm 2. \qquad (13)$$

For $\Delta J = 0$, the Raman displacement is zero and the frequency of the spectrum emission line is the same as that of the exciting light. In effect, this is a kind of scattering process and is in fact just the familiar Rayleigh scattering phenomenom. For $\Delta J = \pm 2$, the displacement is

$$\Delta\nu = F(J+2) - F(J) = \left.\begin{cases} B(J+2)(J+3) - BJ(J+1) = \\ 4B(J+\frac{3}{2}) \end{cases}\right\} \text{for } \Delta J = -2 \qquad (14)$$

$$\Delta\nu = F(J-2) - F(J) = \left[\begin{matrix} B(J-2)(J-1) - BJ(J+1) = \\ -\ 4B(J-1/2) \end{matrix}\right] \text{for } \Delta J = +2 \qquad (15)$$

The series of rotational lines for which $\Delta J = \pm 2$ form what are called S and O branches respectively.

Diatomic molecules in practice are neither ideal harmonic oscillators nor rigid rotors. Hence, the observed spectral transitions do not correspond exactly to the expressions given in the preceding discussion. We shall therefore consider an anharmonic oscillator and a nonrigid rotator model.

For an anharmonic oscillator where higher powers of $x(= r-r_e)$ are used in the expression for the potential energy, the solution of the wave equation gives for the term value

$$G(v) = \omega_e (v + 1/2) - \omega_e x_e (v + 1/2)^2 + \omega_e y_e (v + 1/2)^3 + \qquad (16)$$

where ω_e is the vibrational frequency and $\omega_e x_e$, $\omega_e y_e$, etc., are anharmonicity constants that are very small compared to ω_e. The energy levels of the anharmonic oscillator are not separated by equal intervals; however, the anharmonicities are small except for very light molecules such as light element hydrides.

Considering the separation of successive levels and neglecting cubic terms, one has

$$\Delta G_{v+1/2} = G(v+1) - G(v) = \omega_e - 2\omega_e x_e - 2\omega_e x_e v. \quad (17)$$

$$\Delta^2 G_{v+1} = \Delta G_{v+3/2} - \Delta G_{v+1/2} = -2\omega_e x_e \quad (18)$$

The above equation thus gives a measure of the anharmonicity as well as the zero-th order vibrational frequency ω_e in any given electronic state; therefore, the vibrational constants ω_e and $\omega_e x_e$ can be calculated from the observed infrared bands by calculating the first differences and second differences. If terms involving $\omega_e y_e$ and $\omega_e z_e$ are also included by considering the third and fourth differences of the forms

$$\Delta^3 G_{(v+3/2)} = \Delta^2 G_{(v+2)} - \Delta^2 G_{(v+1)} \quad (19)$$

and

$$\Delta^4 G_{(v+2)} = \Delta^3 G_{(v+5/2)} - \Delta^3 G_{(v+3/2)}, \quad (20)$$

one calculates the anharmonicity constants $\omega_e y_e$ and $\omega_e z_e$.

The rotational term value for a vibrating rotator is derived by including a centrifugal distortion term involving the distortion constant D_v which is much smaller than

B_v. The nonrigid rotator term value may be written

$$F(J) = B_v J(J+1) - D_v J^2(+1)^2 \qquad (21)$$

where B_v is the rotational constant $h/(8\pi^2 c\mu r_e^2)$. D_v is usually of the order of $10^{-4}B_v$ and contributes only a small correction. Therefore, in most cases the second term is negligible. Thus, the frequency of a transition involving a change in the electronic, vibrational, and rotational states, is given by a general expression of the form

$$\nu = T' - T'' = (T_{e'} - T_{e''}) + (G_{v'} - G_{v''}) + F_{J'} - F_{J''}) \qquad (22)$$

The selection rules for the vibrational structure are such that any vibrational state of one electronic state can combine with any vibrational state of another electronic state. That is, in electronic transitions there is no Δv selection rule, and v' and v'' may be any positive integer. However, for the rotational structure the selection rule for J is

$$\Delta J = J' - J'' = 0, \pm 1 \qquad (23)$$

Depending on ΔJ, the lines are grouped in series (branches) as follows for a particular vibrational transition from v' to v":

$$\Delta J = +1, \text{ R branch}, \quad \nu = \nu_e + \nu_v + F_{v'}(J+1) - F_{v''}(J) = R(J) \qquad (24)$$

$$\Delta J = 0,\ Q \text{ branch},\ \nu = \nu_e + \nu_v + F_{v'}(J) - F_{v''}(J) = Q(J) \qquad (25)$$

$$\Delta J = -1,\ P \text{ branch}.\ \nu = \nu_e + \nu_v + F_{v'}(J-1) - F_{v''}(J) = P(J) \qquad (26)$$

in the above relations $\nu_0 = \nu_v$ is called the band origin or null line. Therefore, from the observed transitions, one can in principle calculate the electronic energy T_e, the vibrational frequencies ω_e, anharmonicity constants, and the rotational constants B_v and D_v for the molecular system. It is to be remembered that depending on the energies involved, in order to evaluate the above quantities, the molecular system has to be studied using appropriate ultraviolet, visible, and infrared regions of the spectrum.

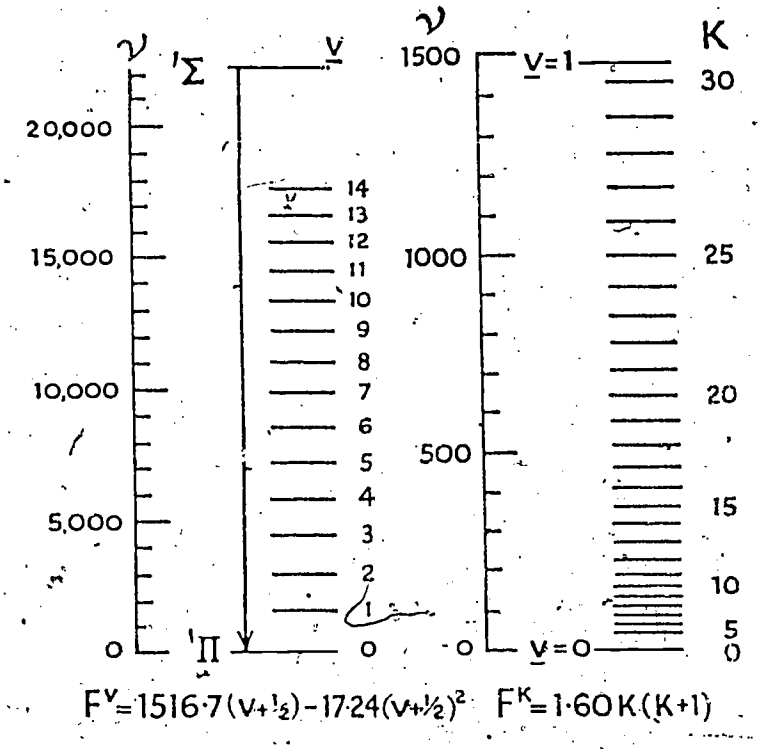

Figure 6. Angstrom Bands of CO

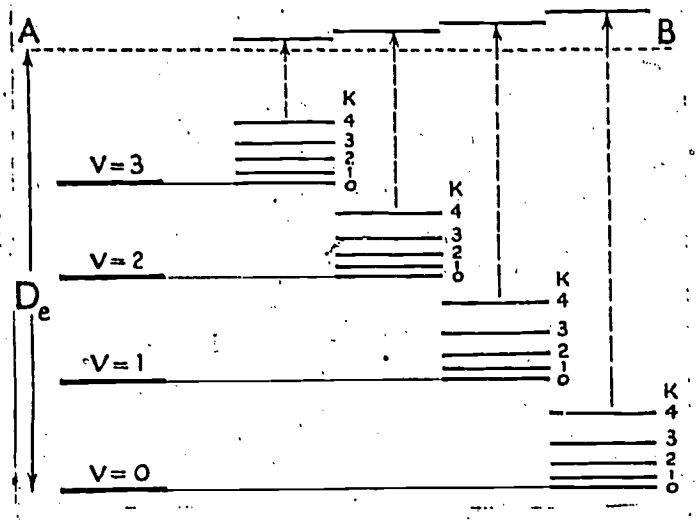

Figure 7. Vibration-Rotation Levels

Fortrat Diagram

The series of lines belonging to the positive branch (R branch) and the negative branch (P branch) can be represented by

$$\nu = c + dm + em^2 \qquad (27)$$

where c, d, e are constants and m is an integer. The graphical plot between ν and m is the Fortrat Parabola (Fig. 3) with the vertex of the parabola showing a "turning back" of one of the branches (m positive is the R branch and m negative is the P branch). Notice the abscissae for

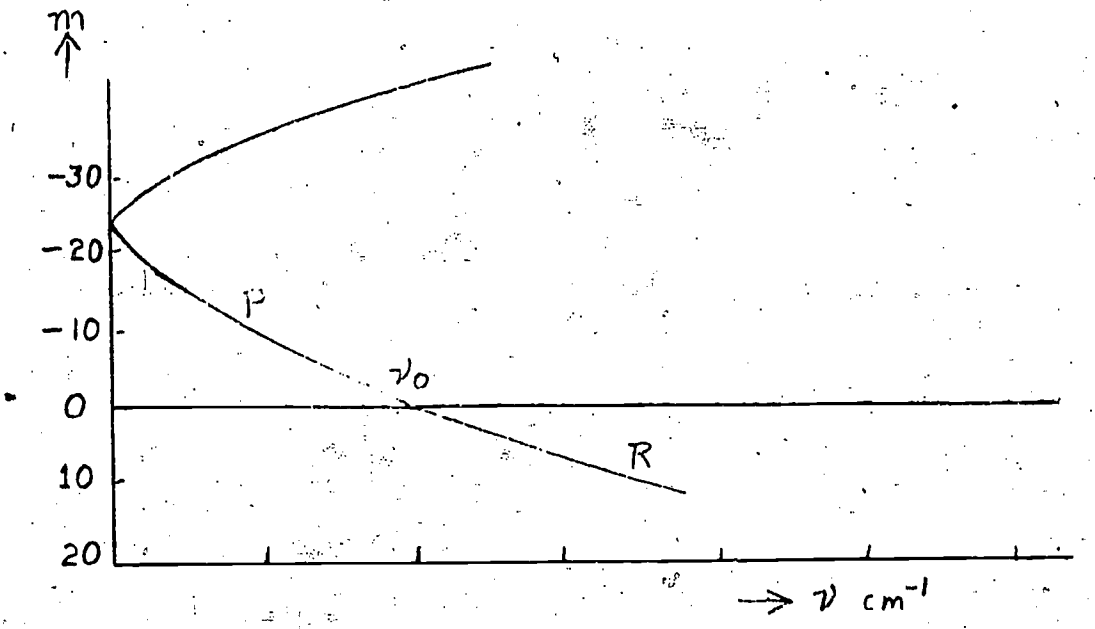

Figure 8. Fortrat Parabola

m = 0 gives ν_0. The "turning back" corresponds to the formation of a "band head".

If $B_{v'} > B_{v''}$, the band head lies in the P branch and there is shading (degrading toward violet (or shorter wavelengths). When $B_{v'} < B_{v''}$, the shading (degrading) is towards red (or longer wavelengths) and the band head lies in the R. Branch. The vertex of the parabola corresponds to

$$m = - (B_{v'} + B_{v''})/2 (B_{v'} - B_{v''}) \qquad (28)$$

obtained by using a single formula of the type

$$\nu = \nu_o + (B_{v'} + B_{v''})m + (B_{v'} - B_{v''})\ m^2 \qquad (29)$$

for the P and R branches. Hence, from the nature of the degrading one can make inferences regarding the relative magnitudes of the rotational constants $B_{v'}$, and $B_{v''}$.

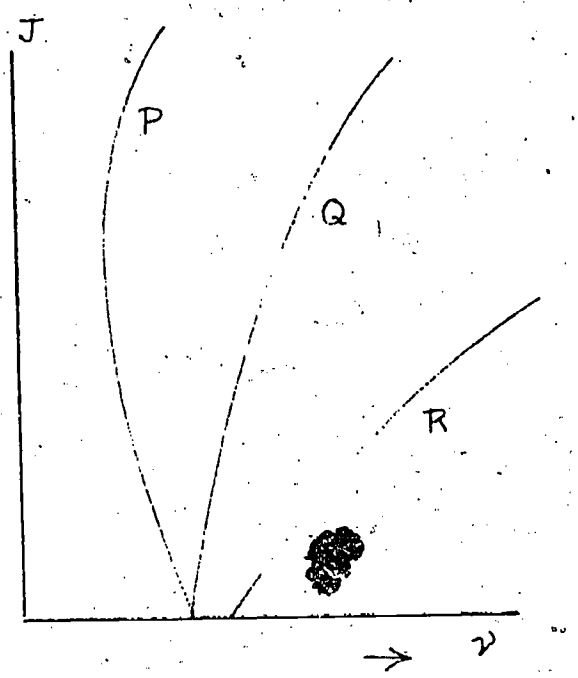

Figure 9. P, Q, R, Branches for the Case $B_{v'} > B_{v''}$ and Degraded to the Violet

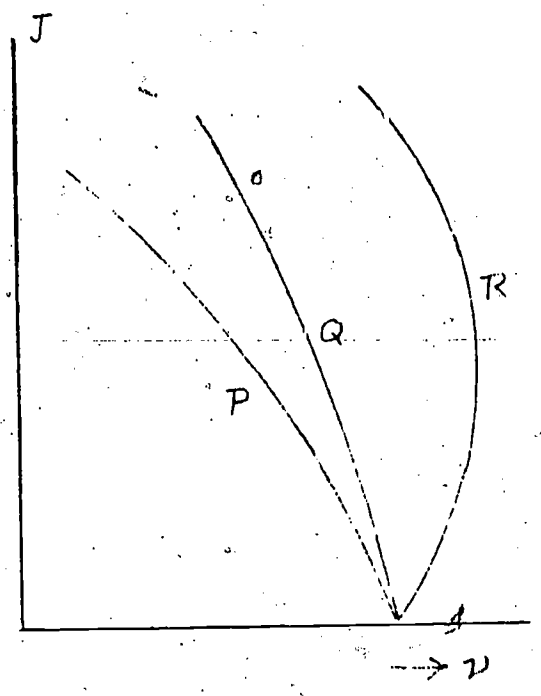

Figure 10. P, Q, R, Branches for the Case $B_{v'} < B_{v''}$ and Degraded to the Red

3. Electronic States and Multiplets

For a given diatomic molecular system AB (see Fig. 6)

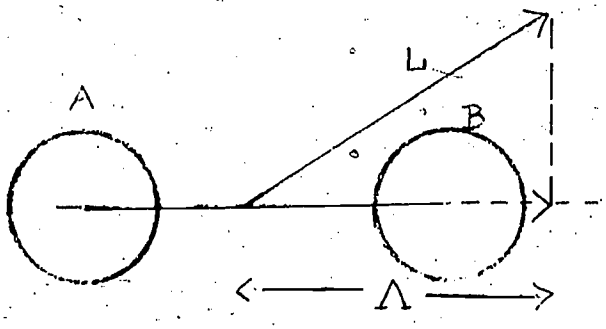

Figure 11. Diatomic Molecule AB and Angular Momentum Component

the electronic orbital angular momentum $\underline{L}$ has a component $|M_L| = \Lambda$ along the internuclear axis. Using Λ, the molecular electronic states are designated Σ, π, Δ, ϕ, etc., according as $\Lambda = 0, 1, 2, 3...$ respectively. This is the analog of the more familiar atomic spectra rotation, s, p, d, f, etc. for $l = 0, 1, 2, 3$. The whole band or the individual lines or both will also show multiplet structure due to the total electron spin S whose component Σ along the internuclear axis can have values S, S-1, S-2,...-S. This is analogous to the values the spin quantum number can have in the atomic case. Thus, as in the atomic case one has $2S + 1$ different values giving the multiplicity of the term. Combining the above factors, a given electronic state is prefixed by the multiplicity $(2S + 1)$ and given a designation indicating Λ value. For example, $^3\Pi$ term corresponds to $\Lambda = 1$ and $S = 1$ and $^2\Sigma$ term has $\Lambda = 0$ and $S = 1/2$. The designations are also preceded by letters A, B, C, X or a, b, c, ...which have usually only historical significance indicating in some cases somewhat the order in which the states were actually discovered. Generally the letter X represents the ground state of the molecule.

$$\Omega = |\Lambda + \Sigma| \qquad (30)$$

This is the analog of the quantum number M_J in the atomic case where $\vec{J} = \vec{L} + \vec{S}$ in the L - S coupling case. There are 2S+1 different values of Ω giving somewhat different energies for the molecular states if $\Lambda = 0$ no Λ- splitting occurs. The general expression for the term value T_e for a multiplet term is

$$T_e = T_o + A\Lambda\Sigma \qquad (31)$$

where T_o is the value neglecting spin. The constant A is referred to as the coupling constant which increases with the number of electrons in the molecule. The positive values of A give rise to normal terms while the negative values correspond to inverted terms.

4. Symmetry Properties of the Wavefunctions

In designating molecular states, the symmetry elements play a significant part. The symmetry properties of the electronic wavefunctions, ψ_e in Eq. (5) and of the rotational levels ψ_r in Eq. (11) have to be considered for this purpose. For the first part, let us take into account the symmetry properties of the field in which the electrons move. There are two symmetry elements viz., a reflection plane containing the internuclear axis and a center of symmetry if the molecule has two nuclei of identical charge. With respect to the first element (plane of symmetry), the wavefunction may or may not change sign on reflection at the plane at symmetry. If reflection in a plane containing the internuclear axis is considered and the electronic wavefunction does not change sign, the state is designated (+). On the other hand, it is classified as a negative (-) state if the wavefunction changes sign. Thus, for example, depending on the effect of a reflection operation one gets Σ^+ or Σ^- states. In the case of identical charges on the nuclei comprising the molecule, there is also the symmetry element called the "center of symmetry" and the electronic states are labelled with g or u as subscripts indicating that the eigenfunctions either remaing unchanged or change sign on "inversion" or that they are even (g) or odd (u). Therefore, the states are designated Σ_g^+ or Σ_u^- or Π_g, Π_u, and so on. In the

g|u inversion x→-x, y→-y, z→-z, (xyz) being the electron coordinates. The electronic states g+ and u- are symmetrical while g- and u+ are antisymmetrical with respect to the exchange of nuclei.

The total wavefunction may be written as

$$\psi = \frac{1}{r} \psi_e \psi_v \psi_{rot} \qquad (32)$$

where ψ_e and ψ_{rot} are the nuclear vibrational wavefunction and the rotational wavefunction respectively. The signs of the resulting wavefunction ψ in relation to the signs of ψ_e and ψ_{rot} are shown in Table 1. (+) for ψ denotes even parity while (-) denotes odd parity.

Table 1.

ψ_e Positive			ψ_e Negative		
J	ψ_{rot}	ψ_v	J	ψ_{rot}	ψ_v
0	+	+	0	+	-
1	-	-	1	-	+
2	+	+	2	+	-
3	-	-	3	-	+
4	+	+	4	+	-
5	-	-	5	-	+

5. Selection Rules for Electric Dipole Transitions

The preceding discussion on the symmetry properties

would be incomplete without a summary of the selection rules governing the electric dipole transitions between molecular states. In a sense the atomic spectral selection rules may be carried over to the molecular case with necessary additions. For electronic states alone, the allowed transitions are given by

Molecular Rule	Analogous Atomic Rule	
$\Delta\Lambda = 0, \pm 1,$	$\Delta L = 0, \pm 1$	(33)
$\Delta\Omega = 0, \pm 1, \Delta J\ 0 \not\leftrightarrow 0$		(34)
$\Delta S = 0,$	$\Delta J = 0, \pm 1$ ($0 \not\to 0$ being forbidden)	(35)
$\Delta\Sigma = 0,$	$\Delta S = 0$	(36)

In addition, for homonuclear molecules, the addition selection rule is that only g $\leftrightarrow$ u transitions are allowed. For the actual rotational levels, the transitions are allowed between positive and negative states with the additional restriction that for homonuclear molecules only symmetric $\leftrightarrow$ symmetric and antisymmetric $\leftrightarrow$ antisymmetric transitions are allowed. Table 2 summarizes the allowed electronic transitions

Table 2.

Heteronuclear Molecules	Homonuclear Molecules
$\Sigma^{\pm} \leftrightarrow \Sigma^{\pm}$	$\Sigma_g^{\pm} \leftrightarrow \Sigma_u^{\pm}$
$\pi \leftrightarrow \Sigma^{\pm}$	$\pi_g \leftrightarrow \Sigma_u^{\pm}$
$\pi \leftrightarrow \pi$	$\pi_u \leftrightarrow \Sigma_g^{\pm}$

$\pi \leftrightarrow \Delta$

$\Delta \leftrightarrow \Delta$

$\pi_g \leftrightarrow \pi_u$

$\pi_g \leftrightarrow \Delta_u$

$\pi_u \leftrightarrow \Delta_g$

$\Delta_g \leftrightarrow \Delta_u$

6. Intensities in Molecular Spectra

The most important and interesting problem in molecular astrophysics is that relating to intensities in the spectra of molecules and the information to be derived from the intensities. As a first step, we will analyze the basic quantum mechanical principles that govern the intensity of a spectral line in absorption or emission of a diatomic molecular system. In this connection, let us examine the transition between two electronic states using the appropriate potential energy curves as shown below and the Franck-Condon principle explaining the intensity distribution in molecular bands.

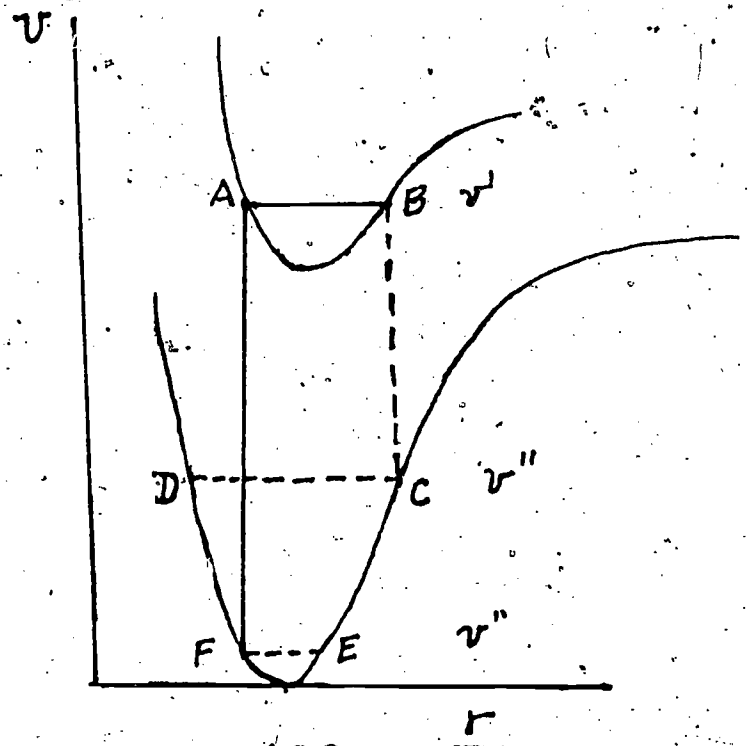

Figure 12. Franck-Condon Principle

During an electronic transition, the electron jump is so rapid compared to the vibrational motion that the relative positions of the nuclei before and after the transition (jump) are nearly the same. The above idea is referred to as the Franck-Condon principle which was originally proposed by Franck and subsequently given a quantum mechanical basis. In a qualitative way the intensity distribution can be explained if one considers the relative positions of the minima of the two electronic states involved. If the minima of the potential energy curves are such that they correspond to the same internuclear distance (the minimum of the upper state being vertically above the minimum of the lower state) as in Fig. 12, the transition v' = 0 to v" = 0 will have the maximum intensity. Other transitions like 1 - 0, 2 - 0, . . . will have rapidly decreasing intensities compared to the intensity of 0-0 band (See Herzberg, Spectra of Diatomic Molecules pp. 195-197)

If r_e values corresponding to the minima of the potential energy curves for the two electronic states involved in the transition are different, the transition 0-0 does not conform to the most probable one according to Franck-Condon principle. In such a case, the 0-0 transition will not have the maximum intensity. For $r_e' > r_e''$, the most intense transition will be from v" = 0 to some value of v' > 0 in absorption and for emission it will be from v'=0

to v">o. Such a qualitative discussion of the intensity distribution in electronic bands is also entirely consistent with the quantum mechanical formulation of the transition probability.

For a transition between v' and v", the probability is given by

$$R = \int \psi' * \vec{M} \psi'' \, d\tau \qquad (37)$$

where $\vec{M}$ is the electric moment ($=\vec{M}_e + \vec{M}_n$) made up of the electronic component $\vec{M}_e$ and the nuclear component $\vec{M}_n$. The The wavefunction ψ itself is the product of the electronic wavefunction ψ_e and the vibration wavefunction ψ_v. Substituting for $\vec{M}$ the quantity $\vec{M}_e + \vec{M}_n$, one gets

$$R = \int \psi_e' * \vec{M}_e \; \psi_e'' \; \psi_{v'} \, \psi_{v''} \, d\tau + \int \vec{M}_n \; \psi_{v'} \, \psi_{v''} \, d\tau_n$$
$$\int (\psi_e' *) \cdot (\psi_e'') d\tau_e \qquad (38)$$

Due to the orthogonality of ψ_e' and ψ_e'', the second factor in Eq. (38) reduces to zero and the transition moment becomes

$$R = \int \psi_e' * \vec{M}_e \; \psi_e'' \, d\tau_e \int \psi_{v'} \, \psi_{v'} \, \psi_{v''} \, dr \qquad (39a)$$

$$= \bar{R}_e \int \psi_{v'} \, \psi_{v''} \, dr \qquad (39b)$$

In the above equation, $\bar{R}_e$ is an average value of R_e which is assumed to vary very slowly with the internuclear distance r. Thus, the intensity in emission or absorption will

be proportional to R^2 and to the populations $N_{v'}$ and $N_{v''}$ respectively. Hence,

$$I \text{ (emission)} \propto N_{v'} R^2 \tag{40a}$$

and

$$I \text{ (absorption)} \propto N_{v''} R^2 \tag{40b}$$

From the preceding discussion, the intensities of the transitions are proportional to the square of the electronic transition moment R_e and to the square of the integral $\int \psi_{v'} \psi_{v''} dr$. We can write for a given band

$$\text{Int.} \propto R_e^2 \left[\int \psi_{v'} \psi_{v''} dr\right] \tag{41}$$

and the quantity

$$q_{v'v''} = \left[\int \psi_{v'} \psi_{v''} dr\right]^2 \tag{42}$$

is called the Franck-Condon factor (FC factor); it is the square of the "overlap" integral involving the vibrational wavefunctions of the two states. Assuming a knowledge of the electronic transition probability R_e^2 one can calculate the relative intensities of the bands from the vibrational "overlap" intergrals.

For purposes of evaluating the vibrational wavefunctions one has to solve the wave equation using an appropriate form for the potential energy, U(r), for the diatomic molecular system. Empirical forms for the functions U(r) have been proposed by several authors.[3] Many of the proposed functions do not give solutions for ψ in closed forms

or in a relatively simple form to calculate the "overlap" integrals easily. However, the most useful one is the simple analytical form proposed by Morse[4] using three parameters. It is of the form

$$U(r) = D_e (1-e^{-\beta x})^2 \qquad (43)$$

where D_e is the dissociation energy referred to the minimum and $x = (r-r_e)$ is the displacement from the equilibrium internuclear distance. β is related to the vibrational frequency ω_e in the particular electronic state and μ_A is the reduced mass of the molecule in atomic mass units according to

$$\beta = 1.2177 \times 10^7 \ \omega_e \sqrt{\mu_A / D_e} \qquad (44)$$

The Morse function has been applied with remarkable success in calculating the vibrational wavefunctions and the Franck-Condon factors. Fig. 13 shows the potential energy curves drawn for the ground state of hydrogen using actual experimental data (continuous curve) and the Morse function (broken curve). It can be seen that the Morse curve is quite a good approximation even for high quantum numbers. Tables of Franck-Condon factors have been provided by several investigators for a large number of molecular systems of astrophysical significance.

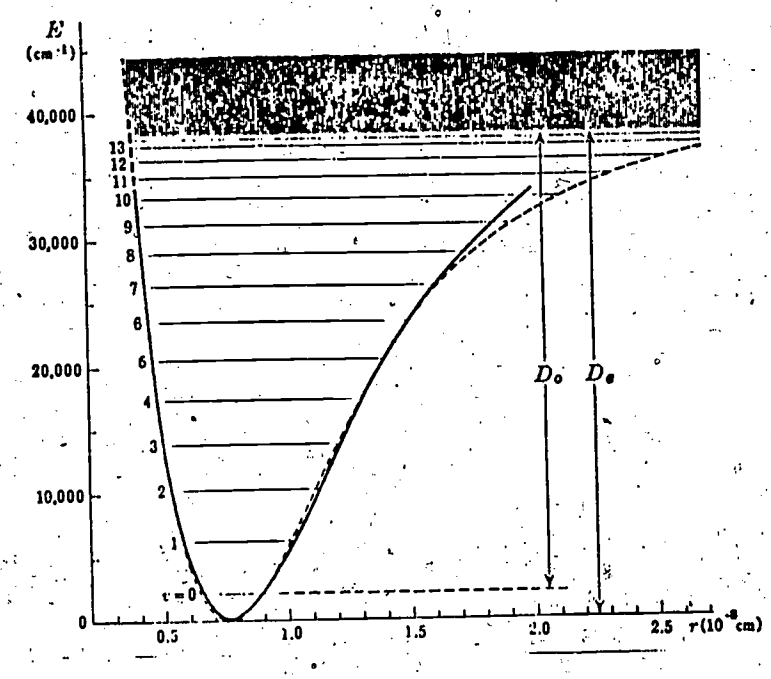

Figure 13. Typical Potential Curve and Vibrational Levels

In the expression for the intensity we have so far considered only the electronic transition moment (R_e) and the vibrational structure accounted for in the form of overlap integrals from which Franck-Condon factors $q_{v'v''}$ are calculated. However, for a complete treatment of intensities it is necessary to include a factor to account for the relative intensities of the rotational lines. The complete line strength then becomes the product of three factors and is

$$S^{nv'J'\Lambda'}_{mv''J''\Lambda''} = R_e^2 \, (\bar{r}_{v'v''}) \; q_{v'v''} \; S^{J'\Lambda'}_{J''\Lambda''} \qquad (45)$$

$S^{J'\Lambda'}_{J''\Lambda''}$ is the so-called Hönl-London factor which represents the individual rotational line. (See Herzberg, Spectra of Diatomic Molecules, p. 208).

7. Transition Probability and Einstein Coefficients

The emission and absorption of radiation are determined by the Einstein's coefficients of transition probability. Consider the molecular system undergoing a transition from one

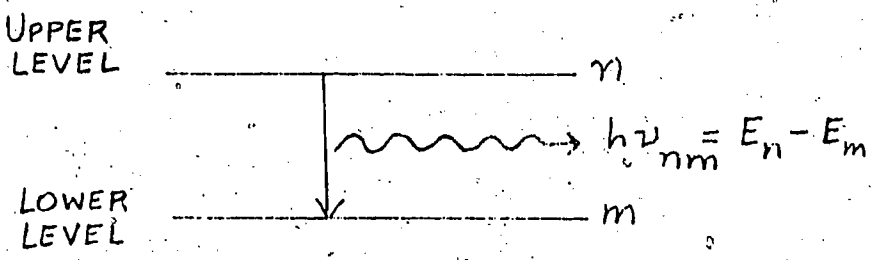

Figure 14. Transitions Between Bound States

energy level E_n to another energy level E_m with the emission of the photon $h\nu_{nm}$. The fraction of the molecules in state n experiencing a transition to state m in one second is denoted by the quantity A_{nm} called the Einstein transition probability for spontaneous emission. The intensity of the photon emission is

$$I_{em} = N_n A_{nm} h\nu_{nm} \tag{46}$$

where N_n is the population of level n. The expression for A_{nm} from quantum mechanics is

$$A_{nm} = \frac{64\pi^4 \nu_{nm}^3}{3hc^3} |R_{nm}|^2 \tag{47}$$

where R_{nm} is the matrix element for the transition moment.

The intensity in emission is therefore

$$I_{em} \propto N_n \nu_{nm}^4 |R_{nm}|^2 \tag{48}$$

Similarly, for absorption of radiation of density P_{nm} by a layer of gas of thickness Δx, the absorption is given by

$$I_{abs} = P_{nm} \quad N_m \quad B_{mn} \quad \Delta x \quad h\nu_{nm} \tag{49}$$

where the quantity B_{mn} called the Einstein coefficient for induced absorption; it is derived from quantum mechanics to be of the form

$$B_{mn} = \frac{8\pi^3}{3h^2C} \quad |R_{nm}|^2 = B_{nm} \tag{50}$$

B_{nm} is called the Einstein coefficient for induced emission. The intensity in absorption is thus proportional to $N_m \nu_{nm} |R_{nm}|^2$.

From the above discussion, it is evident that the intensity of a molecular band in emission or absorption is proportional to the concentration (or population) of radiating or absorbing species in the initial state. The constant of proportionality includes the transition probability A_{nm} or B_{mn} depending on the physical process involved. If one assumes thermodynamic equilibrium for the molecular system at a particular temperature, the populations N_n and N_m of the different vibrational levels are determined by the Boltzmann distribution. Accordingly, if N is the total number of molecules for all practical purposes we have

$$N_n = Ne^{-E_n/kT} \tag{51a}$$

and

$$N_m = Ne^{-E_m/kT} \tag{51b}$$

Thus, the most important application of the study of the intensity distribution in the observed stellar spectra is the determination of the number of molecular emitters or absorbers or the abundances of the molecules.

8. Photometry of Molecular Bands and Temperature Determinations.

The preceding discussion on the intensity distribution in a molecular band system is also of direct use in estimating the temperatures of stars, sun, planets, earth's atmosphere, and interstellar space. Such temperature determinations depend on the photometry of the molecular bands. Let us consider the use of the intensity of the vibrational bands of a band system to obtain the "vibrational temperature" and the intensity distribution amongst the rotational lines for a "rotational temperature" of the system.

For all transitions from a given level v' in the upper electronic state to level v" in the lower electronic state, using the intensities in emission

$$\Sigma_{v"} [I_{em}(v'v")/\nu^4] \propto N_{v'}, \qquad (52)$$

and similarly for the absorption case, we have

$$\Sigma_{v'} [I_{abs}(v"v')/\nu] \propto N_{v"} \qquad (53)$$

where $N_{v'}$ and $N_{v"}$ are the populations of the upper and lower levels respectively. As mentioned earlier, if thermal equilibrium is assumed, the population N_v of an initial

state v is proportional to the Boltzmann factor exp [$-G_o$ (v)hc/kT]. For the term value of the upper level one has

$$\log \Sigma_{v''} [I_{em}(v'v'')/\nu^4] = C_1 - G(v') \, hc/kT, \qquad (54)$$

and similarly for the term value

$$\log \Sigma_{v'} [Iabs(v'v''/\nu] = C_2 - G(v'') \, hc/kT \qquad (55)$$

C_1 and C_2 are constants. One can therefore plot the logarithms of the sums of the 'band strengths' in various v" or v' progressions against the vibrational term values G(v"). Such plots yield straight line relationships as shown in Fig. 15 with the slopes giving a value for hc/kT and thus a "vibrational temperature."

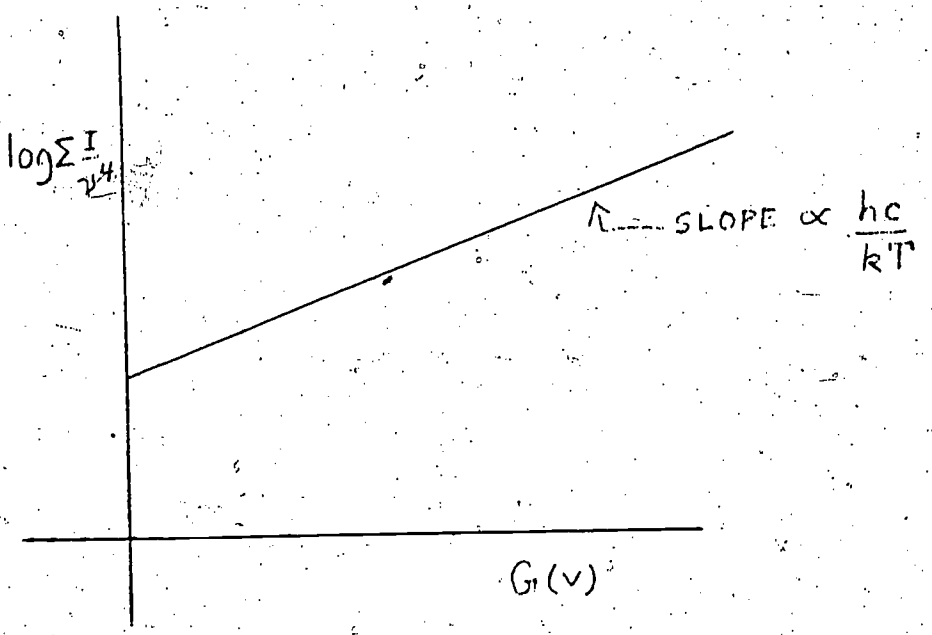

Figure 15. Vibrational Temperature from Slope

It must be clearly understood that the term "band strength" in this case is defined as $(I_{em}(v'v")/\nu)$. In order to obtain reliable results the intensities of all the bands in the progression must be used. Also, the excitation is assumed to be purely thermal. If the intensities of only a few of the bands are known, one can use the Franck-Condon factors and, using the fact that

$$\text{(Band strength/FC factor)} \propto N_{v'} \tag{56}$$

a vibrational temperature can still be deduced.

A procedure similar to the one described above may be used to determine the "rotational temperature" of the emitting or absorbing gas. The dependence of the intensity of the lines in a rotation-vibration band on the rotational quantum number J is described by the thermal distribution according to the relation (See Herzberg, Spectra of Diatomic Molecules, p. 125)

$$N_J \propto N\,(2J+1)\,e^{-E/kT} \tag{57}$$

where N is the total number of molecules, E is the energy of the particular state of the molecule, and (2J + 1) is the statistical weight of the level J. For example, N_J is the population of the level J of the lowest vibrational state if E represents only the rotational energy F (J). If one considers the higher vibrational levels then the population will be determined by using the Boltzmann factor $e^{-E/kT}$

where E is the sum of vibrational energy G(v) and rotational energy F(J), as well as by a factor (J' + J" + 1) using the mean value of (J' + J")/2 for J. In emission, the intensities of lines of rotation or rotation-vibration bands are given by

$$I_{em} \propto N \nu^4 (J' + J" + 1) \exp[-B'J'(J' + 1)hc/kT] \quad (58)$$

and in absorption, the intensity will be

$$I_{abs} \propto N \nu (J' + J" + 1) \exp[-B"J"(J" + 1) hc/kT] \quad (59)$$

where N is the total number of molecules in the initial vibrational level and B' or B" are the rotational constants of the molecule in the upper and lower states, respectively. From these one obtains equations involving $\log[I/(J' + J" + 1)]$ in the forms

$$\log\left(\frac{I_{em}}{J'+J"+1}\right) = \text{Constant} - B_{v'} J'(J' + 1)\, hc/kT \quad (60)$$

and

$$\log\left(\frac{I_{abs}}{J'+J"+1}\right) = \text{Constant} - B_{v"}\, J"(J"+1)\, hc/kT \quad (61)$$

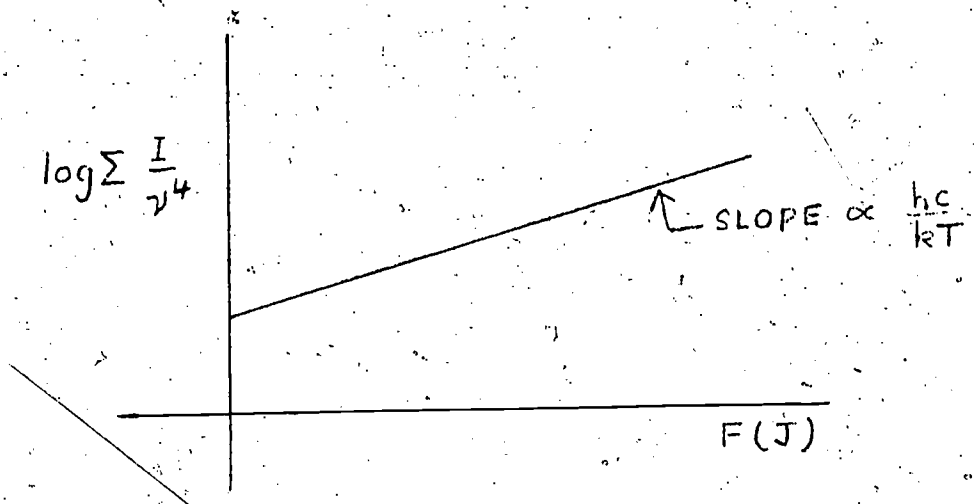

Figure 16. Rotational Temperature

Using a procedure similar to the case of the determination of the vibrational temperature, one can use the emission or absorption intensity and plot $\log[I/(J' + J'' + 1)]$ or $J''(J'' + 1)$ to get the factor Bhc/kT from the slope. Thus, a "rotational temperature" may be deduced from the intensity distribution in the rotational lines of the system. Again, it must be emphasized that the temperature thus obtained will depend on the validity of the assumption that the excitation is purely thermal, for, only then will the populations of the levels be governed by the Boltzmann factor and the statistical weights. For higher J values, the effects of centrifugal stretching become important, and the plot should be $\log[I/(J'+J''+1)]$ versus $F_v(J)$ instead of against $J(J + 1)$ as mentioned above.

The following solar temperatures have been deduced from from rotational intensity distributions in various molecular band systems (See J. A. Hynek, Astrophysics, McGraw-Hill Book Company, Inc., New York, 1951,

From CN	$T_{rot} = 4464° \pm 117°$
From CH	$T_{rot} = 4368° \pm 193°$
From C_2	$T_{rot} = 4871° \pm 304°$
From NH	$T_{rot} = 4658° \pm 234°$
From OH	$T_{rot} = 4773° \pm 104°$

While these temperatures from molecular spectra are in fair agreement with those deduced from atomic spectra

(for example from Fe lines it is 4900° ± 125° and from Ti lines it is 4550° ± 125°), one can see the wide variations in values and error limits. Also, the vibrational" and "rotational" temperatures deduced from the spectra of the same molecular system themselves do not agree closely well because of the limitations of the validity of the assumption of thermal equilibrium. It is therefore necessary to use the temperatures obtained from the above methods with caution in interpreting the observed spectra for determining the abundances, isotope ratios, etc. especially in variable stars (cepheids for example). If thermodynamic equilibrium strictly holds, the "vibrational" "rotational" temperatures should be equal and also agree with the temperatures deduced from atomic lines.

9. Isotope Effects in Molecular Spectra

There are two types of isotopic shifts that are observable in molecular spectra and they can be used to advantage in estimating the concentration ratios of specific elements in stellar sources since isotope shifts for molecular vibration-rotation bands are much larger than for atomic lines. The vibrational isotope effect is that which manifests itself in the shift of the vibrational frequency of the diatomic molecule considered as a harmonic oscillator. It was pointed out earlier that the oscillatory frequency of the molecular vibration is given by

$$\nu = \frac{1}{2\pi}\sqrt{\frac{k}{\mu}} \tag{62}$$

where k is the force constant in the given electronic state and μ is the reduced mass of the molecule. If a pair of isotopic molecules like $C^{12}O$ and $C^{13}O$ are considered to have reduced massed μ and μ_i respectively, the ratio of the frequencies is

$$\frac{\nu_i}{\nu} = \sqrt{\frac{\mu}{\mu_i}} = P, \tag{63}$$

where the subscript i is used for the quantities for the isotopic molecule. The term values describing the vibrational levels of the two types of molecules are

$$G(v) = \omega_e (v+1/2) - \omega_e x_e (v+1/2)^2 + \omega_e y_e (v+1/2)^3 \ldots \tag{64a}$$

and

$$G^i(v) = \omega_i (v+1/2) - (\omega_e x_e)_i (v+1/2)^2 + (\omega_e y_e)_i (v+1/2)^3 + \ldots \tag{64b}$$

$$= P\omega_e (v+1/2 - P^2\omega_e x_e (v+1/2)^2 + P^3\omega_e y_e (v+1/2)^3 + \ldots \tag{64c}$$

Schematically the vibrational levels are shown in Fig. 17.

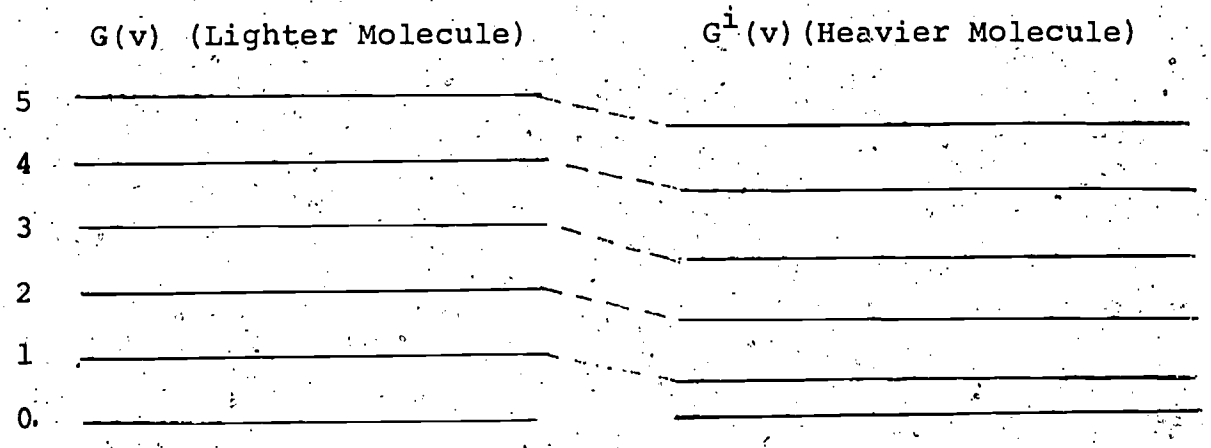

Figure 17. Term Values of a pair of Isotopic Molecules

The differences will be more pronounced if P is much different from the value of 1. The separations increase with the quantum number v. Neglecting terms higher than quadratic in v, the isotope shift $\Delta\nu$ is calculated to be

$$\Delta\nu=\nu-\nu^{i} = \omega_e(1-P)v-\omega_e x_e(1-P^2)v-\omega_e x_e(1-P^2)v^2\approx(1-P)v\Delta G_{v+1/2} \quad (65)$$

Similar to the vibrational isotopic effect, there is also a shift in the rotational lines of a diatomic molecular spectrum. Since the rotational spacings are determined by the rotational constant $B = h/8\pi^2 c\mu r_e^2$, the rotational term values for a pair of isotopic molecules will be given by the relations

$$F = BJ\ (J+1) \quad (66)$$

and

$$F_i = B_i\ J(J+1) = P^2BJ(J+1) \quad (66a)$$

The rotational levels of two isotopic molecules are shown schematically in Fig. 18. The separations increase with J and the lighter molecule has larger separations. Neglecting

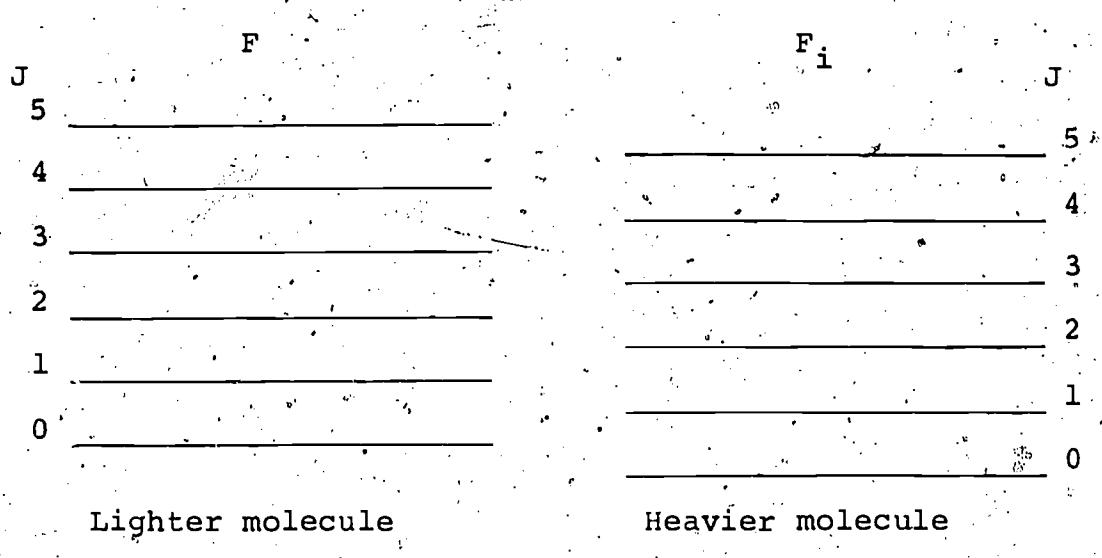

Figure 18. Rotational Spacings of two Isotopic molecules

the interaction of rotation and vibration, one has for the rotational isotopic shift

$$\Delta\nu_r = \nu - \nu_i = (1-P^2)\ [B_e' J'(J'+1) - B_e'' J''(J''+1)] \qquad (67a)$$

$$= (1-P^2)\ \nu_r \qquad (67b)$$

where ν_r is the frequency of the rotational line for the molecule.

Using the above equations for the shifts and the relative intensities of the isotopic molecular lines, the abundance ratio of isotopes can be estimated. For example the Swan bands of C_2 and the violet bands of CN have been used to determine the ratio of C^{13} to C^{12}. The same method has been used for obtaining C^{13}/C^{12} ratio from the CO lines observed in stellar spectra. The ratio of C^{13}/C^{12} is found to be 1/4 in some carbon stars while some others have a ratio similar to that on earth. Such studies of the abundance ratios of isotopes are significant for a proper understanding of the nuclear processes and energy generation in stars.

10. Polyatomic Molecules in Stellar Sources

Although the entire discussion so far has centered only on diatomic molecular species in stellar sources and the applications of the spectra for determing temperatures, physical processes etc. in the sources, a study of molecular astrophysics should also survey briefly the presence of polyatomic

molecules in various sources. Lines of several polyatomic molecules like N_2O(7.78μ band), CH_4(1.67μ band), and NH_3 (2.0μ band) have been observed in the solar spectrum. Rotation-vibration bands of CO_2, CH_4, NH_3 have been found in the spectra of planets like Venus, Jupiter, and Saturn. The study of these bands and their intensities have led to the determination of the abundances of the molecules in those planetary atmospheres.

With the renewed surge of activity in radio astronomy, several interstellar molecules like formaldehyde, alcohol, ammonia, etc., have been identified from the pure rotational spectral lines observed in the radio frequency spectrum. From a study of the vibrational spectra and rotation-vibration spectra of many of the polyatomic molecules the rotational distortion constants of the molecules can be calculated and hence pure rotational lines can be derived theoretically. Such theoretical calculations are being used for verifying the presence of many molecules in interstellar space. This is at present a very rapidly growing field of research, and complementary studies in laboratory of the spectra of these molecules are proving to be useful and significant.

MOLECULAR ASTROPHYSICS

REFERENCES

1. G. Herzberg Spectra of Diatomic Molecules, D. Van Nostrand Company, Inc., Princeton, N.J. (1957).

2. G.M. Barrow Introduction to Molecular Spectroscopy, McGraw-Hill Book Company, Inc., New York (1962).

3. R.C. Johnson An Introduction to Molecular Spectra, Pitman Publishing Corporation, Chicago (1949).

GAMMA RAY ASTROPHYSICS

1. Introduction

After more than a decade of intensive studies at several laboratories, the cosmic gamma rays were discovered in the sixties. The various observations like the experiment on OSO-3 satellite which showed that gamma ray photons with energies of the order of 10^{16} times that of the radio waves were emitted from the plane of the Galaxy and many others followed in quick succession. Finally the gamma ray astrophysics has emerged as a full blown observational science and as an important branch of astrophysics to probe the universe. Unlike the charged particles from stellar sources that are deflected by magnetic fields or the neutrons as well as other particles that undergo decay enroute, the gamma rays because of their chargeless state are the only high energy quanta that can reach us from very distant sources without being affected. They can provide a unique and valuable medium for conveying information directly from the regions where the processes are occurring on many of the major energy transfers taking place in the universe.

A number of astrophysical problems including those unique to large scale astrophysical bodies can be studied from analyses of gamma radiation from cosmic sources. Further it enables us to expand our knowledge of the electromagnetic phenomena for diffuse and discrete source X-ray emissions to high energies. Measurements

of gamma ray fluxes are also of significance from the point of view of their relation to the sources of relativistic particles and the theoretical interest associated with their behavior. Taking the example of our own galaxy, the presence of energetic protons within discrete sources and the interactions of high energy nucleons with other nucleons can be studied using the emitted gamma rays so that a complete picture of the dynamics of our galaxy and the origin of energetic particles can be determined. The two processes of (i) nuclear interactions of energetic cosmic radiation with inter-galactic gas and (ii) nucleon antinucleon annihilation result in the characteristic neutral pi meson (π^o) decay gamma ray spectrum which due to the expanding model of the universe experiences a red shift. The study of gamma ray astronomy is thus going to be directly related to the subject of cosmology. The electromagnetic interaction mechanisms of Bremsstrahlung; synchrotron emission, and Compton scattering important in X-ray astronomy are also important in gamma ray astronomy. Also, there are the gamma rays resulting from nucleosyntheses processes in supernovae explosions and shock waves from stellar collapse. The study of the spectral characteristics of such photons would provide the clues to the validity of theories that predict such outbursts. There are thus several problems relating to the studies of gamma ray astrophysics that are of fundamental importance and they include (a) cosmic ray origins, (b) cosmic ray

densities in the galaxy and in intergalactic space, (c) galactic and intergalactic matter densities and magnetic fields and (d) density of antimatter in the universe. In this module therefore, we will first review briefly the mechanisms of gamma ray production, then describe the main features of observational techniques, summarize some of the important results obtained thus far, and comment on the future promise this branch of astrophysics holds in the era of space shuttles.

2. Mechanisms for Production of Cosmic Gamma Rays

The chief processes connected with the origin of gamma rays have been reviewed in detail by several authors[1-3]. There are three distinct categories for us to consider in connection with the production mechanisms. These categories are: (a) gamma ray continuum which constitutes the greater part of cosmic gamma rays, (b) gamma ray line radiation, and (c) gamma ray fluxes from discrete sources. Let us consider these categories and the processes that give rise to the photon flux in each case.

(a) Gamma Ray Continuum: As mentioned earlier, the continuum accounts for a major proportion of the observed flux and the main processes that contribute to the gamma ray continuum are (i) π^0 (neutral meson) decay, (ii) Bremsstrahlung from relativistic electrons, and (iii) Inverse Compton Effect. The neutral π mesons are produced as a result of collisions between electrons, or between protons, or

at very high energies in proton-photon collisions. At low energies, another source of π^0 mesons is the proton-antiproton annihilation. This process that is important at low energies gives a sharp peak at about 70 MeV. The π^0 mesons decay with a lifetime of 10^{-16} seconds according to

$$\pi^0 \rightarrow \gamma + \gamma \tag{1}$$

with energy of each gamma ray at 70 MeV. In the case of proton-proton collisions (the most important source of π^0 mesons) one has for energies of the incident proton in excess of 290 MeV,

$$p + p \rightarrow p + p + n_1(\pi^+ + \pi^-) + n_2\pi^0 \tag{2}$$

$$p + p \rightarrow p + n + \pi^+ + n_3(\pi^+ + \pi^-) + n_4\pi^0 \text{ etc.,} \tag{3}$$

where n_1, n_2, n_3, and n_4 are small integers. Such reactions will occur in interstellar space where interstellar gas which is chiefly hydrogen is bombarded by cosmis ray protons. In proton-photon collisions, π^0 mesons will be produced if the energy of the colliding proton is above the threshold given by

$$E_{PROTON} > \frac{m_\pi}{2\epsilon}\left(m_\pi + 2M\right), \tag{4}$$

where ϵ is the energy of the photon and m_π, M are the masses of the π meson and the proton respectively. For photon with energy 2 eV, E_{proton} should be in excess of 10^{17} eV. For microwave photons,

$E > 10^{20}$eV and gamma rays with energies in the range $10^{18} - 10^{19}$eV will be produced. The Bremsstrahlung process for the production of gamma ray continuum results from the slowing down of relativistic electrons by the Coulomb fields of charged particles. Naturally for this process the gamma ray flux will depend on the spectrum of electron energies and the number of charged particles in the particular region. Theoretical calculations[4] indicate that the fluxes from π^0 meson decay and Bremsstrahlung processes are of the same order of magnitude in the case of galactic and extragalactic radiations. Finally in the Inverse Compton Effect shown schematically in Fig. 1, the relativistic electron e collides with radiation of energy $h\nu$ and an enhancement of the photon takes place resulting in a recoil photon (gamma photon) $h\nu_1$. In

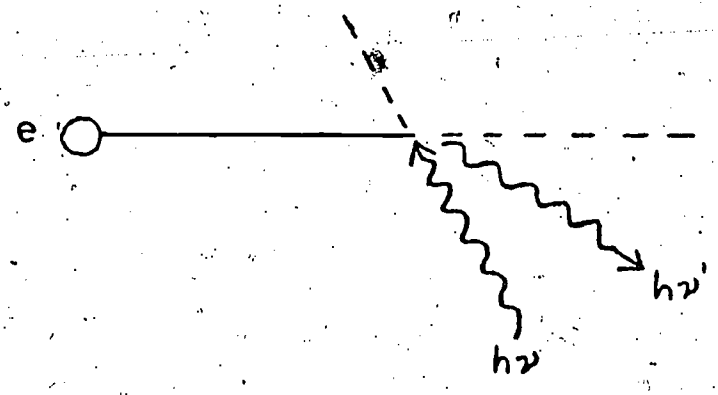

Fig. 1. Inverse Compton Process

this case as one would expect the gamma ray spectrum will depend on the energy spectrum of the relativistic electrons and the (incident) photon density. While electron densities are low in astrophysical situations under consideration, photon densities are relatively high. Again theoretical calculations of the flux from galactic as well as extragalactic origins due to this process have been made and the fluxes are one to two orders of magnitude different from those due to π^0 meson decay and Bremsstrahlung processes.

(b) Gamma Ray Line Emission: Though the gamma ray continuum accounts for a large proportion of cosmic gamma rays, the processes that give rise to line emissions are equally important for a fuller understanding of the conditions in astrophysical phenomena connected with gamma rays. In the realms of low energies (less than 10 MeV) the chief processes giving rise to line emissions are the electron-positron pair annihilation and nuclear reactions like those involving protons and neutrons. The annihilation process

$$e^+ + e^- \rightarrow \gamma + \gamma \qquad (5)$$

gives gamma rays peaked at 0.51 MeV (the rest mass of an electron). The flux will depend on the positron density. The nuclear transitions like

$$p + n \rightarrow d + \gamma \qquad (6)$$

could give gamma rays in 2.23 MeV range. Collisions of cosmic

rays with gas molecules can also result in emission of characteristic gamma rays from excitation of nuclei and these will have fluxes dependent on chemical compositions.

(c) Emissions of Gamma Rays from Discrete Sources: Such emissions hold a much greater promise for unravelling many phenomena connected with the origin and acceleration of electrons in the sources to name just a few. These emissions are particularly notable as we will see later in our discussion on a prime source namely the Crab nebula.

Synchrotron emission and Inverse Compton Processes are considered in relation to discrete sources and comparison of the inferences from gamma ray studies with X-ray and Radio Astrophysics will be one of the most fascinating and challenging developments in astrophysics. With these ideas on the general nature of the processes for gamma ray emissions, we will proceed to discuss some of the details of instrumentation and observational techniques connected with measurements of gamma ray fluxes.

3. Instrumentation in Gamma Ray Astrophysics

The instrumentation and observational techniques depend on a number of factors (as one can expect from the different regions of energy in which the gamma ray emissions are studied) like the sensitivity of the various detectors, the nature of the experiments (whether they are balloon experiments or satellites are to be used), "pay load" considerations, etc. Let us discuss the principles in

the design of some of the common arrangements used in these experiments and summarize briefly the general schematics of the recent development of a high resolution Germanium Gamma Ray Spectrometer.

(a) In the most interesting region of low energy range up to 30 MeV, in order to obtain really interesting results and compare with theoretical predictions, the sensitivity of the technique used is very crucial. The technique adopted here uses a simple detector called Phoswich detector that makes use of two different scintillator materials with also two different scintillation response times. In general, the materials used are an alkali halide crystal and a plastic material. The alkali halide crystal (NaI or CsI) is particularly sensitive to photons while the plastic scintillator is transparent to photons but is a highly efficient detector for charged particles. The alkali halide crystal is surrounded by the plastic scintillator and since the response times of the two materials are different a single photomultiplier can be used with advantage to register the photon event and the particle event both of which can be analyzed with electronic circuitry. The light output of the crystal (assuming it is thick enough to absorb the secondary electron) will be proportional to the incident energy of the gamma rays. Using known sources of gamma rays as calibration standards one can easily estimate the incident flux. For studying discrete sources, where in this region

of energies the Compton process will be dominant, and to study the directional properties it is necessary to use appropriate collimators as in the case of X-ray detectors.

(b) In the medium energy range of 30 MeV to 1 GeV, the observational techniques utilize the results of positron-electron pair production resulting from the incident Gamma rays. Spark chambers or nuclear emulsions are used to plot the trajectories of the products. Since the total energy of the incident gamma rays will be transferred to the positron-electron pair, the energy of the particles e^+ and e^- will be a measure of the incident energy. Usually a lead converter that has a high probability for pair production is employed. In some designs, the metal plates of the spark chamber detector or the silver atoms in the nuclear emulsion detector serve as the medium for pair production. The two diverging tracks of e^+ and e^- within the detector will be used to record the event of incidence of gamma rays and the energies estimated. In this region the general shape of the gamma ray spectrum is important and the technique is also suitable for rough estimates of energies.

(c) A design specially suitable for studying discrete sources of gamma rays and usable at balloon altitudes is shown in Fig. 2. This makes use of several spark chambers, scintillation detectors, and a Cherenkov detector. At heights reached by the balloons with their instrument package the interactions of the cosmic rays with the upper

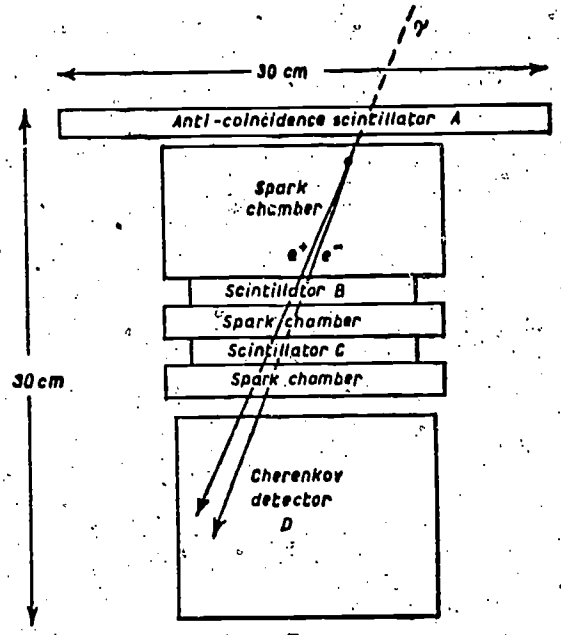

Fig. 2. Detector for Gamma Rays in Balloon-borne Instruments

layers of the atmosphere will result in large flux of the secondary gamma rays. This flux which is an order of magnitude stronger than the flux due to diffuse background will completely mask the latter.

(d) The arrangement used in Explorer XI satellite is shown in Fig. 3. These detectors weigh only about 30 pounds and are best suited for satellite experiments. However, due to lack of visual display arrangement and other factors, these are generally ideal only for setting an upper limit to the diffuse background.

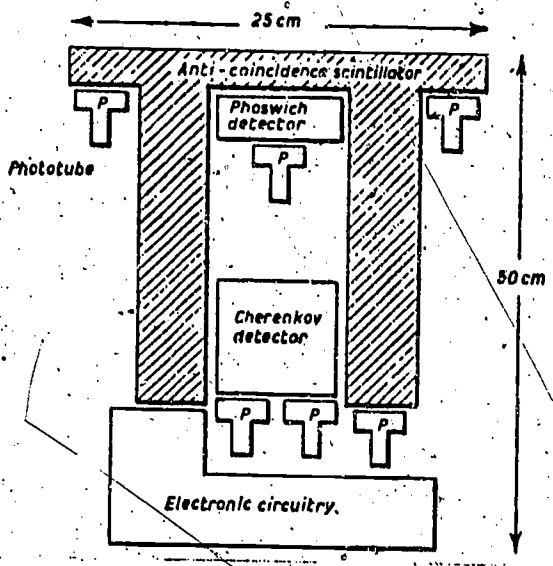

Fig. 3. Gamma Ray Detector
Carried by Explorer XI Satellite

(e) In the high energy range of 1 - 100 GeV and beyond the experiments are very difficult due to the very low fluxes at high energies. The low fluxes require large areas of the detector and the mass of the detector "pay load" is a major consideration for balloons or rockets and the like. However, another design has been developed and used for an indirect observation of such high energy radiation. Above 10^{11} eV, the high energy gamma rays strike the earth's atmosphere and give rise to showers of particles ("air showers"). Such air showers give rise to bursts of Cherenkov radiation which is detectable using ground based equipment in the form of a simple apparatus. The apparatus

will record the intensity and direction of the shower particles or Cherenkov light or both and thus provide the information on the direction and energy of the incident gamma ray photon. The chief advantages are also that a small light detector with special optics can combine a large sensitive area and good angular resolution. There is also the chief disadvantage that the use of the technique is feasible only on clear moonless nights and there is also no anticoincidence counter to subtract the showers generated by charged cosmic ray particles.

Fazio[5] describes such an instrument which consists of a 10 m aperture light reflector with an effective sensitive area of 1.3×10^4 m^2 and effective angular resolution of 1^o. Such a reflector is mounted at the 2300 m level of Mount Hopkins in Arizona. Showers in the range $10^{11} - 10^{15}$ eV can be measured conveniently by the burst of Cherenkov light when the shower particles pass through the atmosphere. The gamma ray sources will be apparent by the increase in shower counting rate when the instrument is in line with the source direction (for fuller details of special optics used at different stations and results refer to Fazio[5]).

(f) The most important and recent development in instrumentation and observational techniques is the Ge(Li) gamma ray spectrometer used in the first satellite experiment. A detailed description is given by Nakano et al.,[6] and the general schematic of the cross-sectional view of the arrangement used is shown in Fig. 4. The Ge(Li) detector with

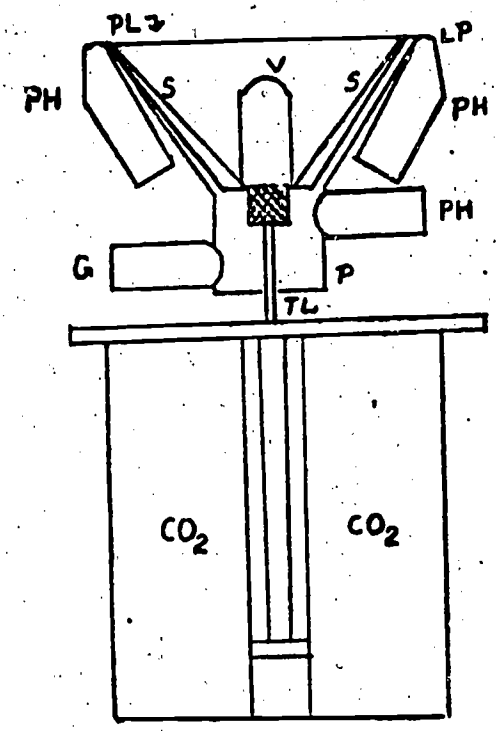

CO_2 - Solid CO_2 to last for ~1 year
TL - Thermal Link
P - Plastic Scintallator
G - Ge(Li) Detector
PH - Photomultipliers
S - High Density Shielding (45° cone)
V - Vacuum Cover
PL - Plastic Scintillator

Fig. 4. Ge(Li) Gamma Ray Spectrometer (Cross-sectional View)

a volume of 60 cm^3 and an active area of 15 cm^2 is thermally linked using copper to a cooler having solid CO_2 (about 35 pounds to last for a year) and maintained at cryogenic temperatures. The operating temperaure of the detector is 130°K. A tungsten shield weighing ~45 pounds is arranged in relation to the view cone as shown. A plastic scintillator anticcoincidence system with four photomultipliers is used (only two of the photomultipliers are shown in the cross-sectional view). The range of energies is 40 keV to ~ 2.8 MeV and the resolution is 3.5 to 4 keV. The pulses from the Ge(Li) detector are

processed by a pulse-height analyzer and stored in an on-board tape recorder for providing data for worldwide experimenters.

Metzger[7] describes two other experimental arrangements in connection with HEAO experiments in the 0.1 to 10 MeV region. These are large scintillator detection systems that can record data in a number of modes and involve sophisticated processing logic as well as a modified Ge(Li) spectrometer in one type. However, it is quite evident that with elapse of time, higher sensitivity and resolution will be the key factors in designing complex detector systems. The interested reader can refer to some of the recent developments outlined in the NASA publications.[5-7]

4. Observational Results

In this section we shall review briefly some of the interesting results from gamma ray experiments and mention the production mechanisms involved in some cases where sufficient evidence has accumulated. The study of various astrophysical phenomena involving gamma ray emission is in its early stages and as such it is preferable to focus our attention to a few of the experiments rather than catalog all of them. Let us start with some of the first satellite experiments using Ge(Li) high resolution gamma ray spectrometer and giving us information on background from electron-positron annihilation and electron bremsstrahlung.

(a) Low Energy Range The first satellite experiment making use

of the high resolution Germanium instrument deserves particular discussion in connection with observations in the low energy range. The Ranger moon rockets series in which experiments were conducted using phoswich detector is also relevant as they determined the upper limits of the intensities of the lines at the 0.51 MeV and 2.23 MeV positions. Using the high resolution germanium gamma ray spectrometers, the most prominent line present in all spectra was found to be 511 keV and the source of this line is concluded to be the electron-positron annihilation. Lack of modulation of the intensity of this line by the spin angle and the comparatively high count rate leads to the inference that apparently significant portion of the radiation is produced on the satellite. In addition to the 511 keV line, smooth backgrounds attributable to electron bremsstrahlung are also commonly encountered in these satellite measurements with Ge(Li) gamma ray spectrometers. The bremsstrahlung backgrounds can come from (i) the radiation belt electrons stopping in the vicinity of the spectrometer and (ii) the electrons precipitating into the earth's atmosphere. Also, during the orbit at a time of high geomagnetic activity, gamma ray counting rates over the polar caps were found to be significantly increased.

(b) Medium Energy Range In the range of 10 MeV to 1 GeV, the experiments conducted with OSO-3 telescope and SAS-2 telescope[8] deserve some discussion in this review. The OSO-3 telescope measured detectable intensities of gamma radiation along the galactic equator at

all galactic longitudes. It was concluded that at least fifty percent of the galactic flux comes from the decay of the neutral π mesons produced in cosmic ray collisions.

Details of instrumentation in SAS-2 experiments and the complete description are given by Kniffen et al.[9] The results obtained by SAS-2 fall into three categories: (i) A weak but finite component of high energy diffuse flux, presumably extra-galactic gamma rays coming from regions other than galactic plane; (ii) High intensity gamma rays coming from the galactic center region and (iii) flux from discrete sources like the flux for the Crab nebula emission. With respect to the diffuse flux, the possible models concerning the origin seem to be the interaction between cosmic rays and interstellar matter and the particle-antiparticle annihilation mechanism. In both models the resulting gamma ray spectrum, which is primarily due to π^0 decay is red shifted to a considerable extent due to the expansion of the universe. The verification of the above models will therefore verify the model of the expanding universe as well.

The SAS-2 experiments also confirmed the observation of galactic plane radiation and the enhanced intensity from the region of the galactic center noted by OSO-3 experiment. That the energy spectrum was not only due to π^0 meson decays was also concluded from SAS-2 experiment since it also revealed the presence of enhanced flux below 70 MeV. Regarding discrete sources data analyses are continuing and with the

higher sensitivity of SAS-2 it should be possible to study in detail a number of such sources and determine upper limits for fluxes from even very weak sources.

(c) High Energy Range As was mentioned earlier, in the range of 10^{11} eV energy, the Cherenkov light detectors are used making use of the "air showers". The search was made in the direction of strong radio sources like Cygnus A, Cassiopeia A, Taurus A (Crab Nebula) and Virgo A as well as several quasars 3C147, 3C192, and 3C273. Nothing was detected. From 1968, the primary source for observation has been the Taurus A in the Crab nebula at the center of which is the pulsar NP 0532 with the shortest period. The nebula shows strong synchrotron radiation in the X-ray, optical, and radio regions and thus a possibility for strong gamma radiation was foreseen. Grindley[10] employing proton shower technique has reported evidence for pulsed gamma rays with energies 6×10^{11} eV from the pulsar occurring at the pulsar period. In addition Fazio et al.,[11] reported also continuous gamma ray flux (with energy greater than 2×10^{11} eV) from the nebula with the flux varying with time and reaching significant amounts 60 to 120 days after a major spin-up of the pulsar NP 0532. A measurement of the gamma ray flux leads to a determination of the average magnetic field which is estimated near 2.5×10^{-4} Gauss. Future work in monitoring the Crab nebula and measurement of the ratio of pulsed to continuum radiation should be extremely interesting. The explanation for

the 60 to 120 days lapse between the pulsar spin-up and the maximum flux should also be equally important. In addition, the other promising sources are the pulsars, the one in Vela supernova remnant and CP 0950 the closest pulsar.[12]

(d) Gamma Ray Emission in Solar Flares The results obtained by the gamma ray detector of Chupp et al.[13,14] in OSO-7 space craft are also interesting since they are connected with observations of gamma ray emissions during solar flares. From the flare of August 4, 1972, four gamma ray lines at 0.51, 2.23, 4.43, and 6.13 MeV have been observed and these are from positron annihilation, neutron capture on hydrogen, and the nuclear excited states of C^{12} and O^{16} respectively. Further studies of these observations and study of solar flares at other wave lengths should lead to a rather specific acceleration and interaction model for these flares.

5. Conclusion

Some remarks about future directions of this new field are in order at this stage. With higher and higher sensitivity of the detectors that are being developed, and with the planned space shuttles, a new era in gamma ray astrophysics or high energy astrophysics in general has opened up. Above 50 or 100 MeV and upwards there is a lot of promise for exciting developments. While the basic physical processes of solar flares are understood in comparison to other production processes, the magnitudes of the solar flares may attract people for the studies in the

future. Even more interesting will be the studies with instruments in space at the time of a supernova explosion and attempts to understand the nucleosyntheses processes in supernovae which at present is a matter of speculation. The observations and analyses of the isotropy of gamma ray flux will be extremely vital for information on cosmological models and this will be another next important step.

GAMMA RAY ASTROPHYSICS

REFERENCES

1. G.G. Fazio, Annual Reviews of Astronomy and Astrophysics 5, 481 (1967).

2. P. Morrison, Annual Reviews of Astronomy and Astrophysics 5, 325 (1967).

3. R.J. Gould, American Journal of Physics 35, 376 (1967).

4. T.C. Weekes High Energy Astrophysics, Chapman and Hall Ltd. London (1969).

5. Gamma Ray Astrophysics, Ed. F.W. Stecker and J.I. Trombka, NASA Goddard Space Flight Center Symposium, April 20, 1973, NASA Publication No. NASA SP-339, P. 153.

6. Ibid, p. 71.

7. Ibid, p. 97.

8. Ibid, p. 139.

9. G.G. Fazio and Y. Pal in X-ray and Gamma Ray Astronomy Proc. IAU Symposium No. 55, Ed. H. Bradt and R. Giacconi, D. Reidel Publishers, Dordrecht, Holland (1973).

10. J.E. Grindley, Astrophysical Journal, Letters 174, L9 (1972).

11. G.G. Fazio et al., Astrophysical Journal, Letters 174, L119 (1972).

12. B.K. Chatterjee et al., Nature (London) 231, 127 (1971).

13. E.L. Chupp et al., Nature (London) 241, 33 (1973).

14. P.R. Higbie et al., IEEE Trans. Nucl. Sci. NS 19, 606 (1972).